[redacted]

[redacted]

X72-10669

NASA TM X-2582

NASA TECHNICAL MEMORANDUM

NASA TM X-2582

LOW-SPEED AERODYNAMIC CHARACTERISTICS OF A MODEL HAVING A 42° SWEPT LOW WING WITH A SUPERCRITICAL AIRFOIL, DOUBLE-SLOTTED FLAPS, AND A T-TAIL

[redacted]

by Paul G. Fournier and William C. Sleeman, Jr.

Langley Research Center
Hampton, Va. 23365

NATIONAL AERONAUTICS AND SPACE ADMINISTRATION • WASHINGTON, D. C. • SEPTEMBER 1972

[redacted]

[redacted]

1. Report No. NASA TM X-2582	2. Government Accession No.	3. Recipient's Catalog No.
4. Title and Subtitle LOW-SPEED AERODYNAMIC CHARACTERISTICS OF A MODEL HAVING A 42° SWEPT LOW WING WITH A SUPERCRITICAL AIRFOIL, DOUBLE-SLOTTED FLAPS, AND A T-TAIL (U)		5. Report Date September 1972 6. Performing Organization Code
7. Author(s) Paul G. Fournier and William C. Sleeman, Jr.		8. Performing Organization Report No. L-8358 10. Work Unit No. 501-15-01-04
9. Performing Organization Name and Address NASA Langley Research Center Hampton, Va. 23365		11. Contract or Grant No. 13. Type of Report and Period Covered Technical Memorandum
12. Sponsoring Agency Name and Address National Aeronautics and Space Administration Washington, D.C. 20546		14. Sponsoring Agency Code

15. Supplementary Notes

16. Abstract

A low-speed wind-tunnel investigation has been made in the Langley V/STOL tunnel to determine the static longitudinal and lateral stability characteristics of a general research model which simulated an advance configuration for a commercial transport airplane with a T-tail. The model had a 42° swept, aspect-ratio-6.78 wing with a supercritical airfoil and a high-lift system which consisted of a leading-edge slat and a double-slotted flap. Various slat and flap deflection combinations represented clean, take-off, and landing configurations. Effects on the longitudinal and lateral aerodynamic characteristics were determined for two flow-through, simulated-engine nacelles located on the sides of the fuselage near the rear of the model.

17. Key Words (Suggested by Author(s))

High-lift flap systems
Supercritical wing
Low-speed aerodynamic characteristics
Transport configuration
Swept wing

19. Security Classif. (of this report)	20. Security Classi
[redacted]	

[redacted]

LOW-SPEED AERODYNAMIC CHARACTERISTICS OF A MODEL HAVING A 42° SWEPT LOW WING WITH A SUPERCRITICAL AIRFOIL, DOUBLE-SLOTTED FLAPS, AND A T-TAIL*

By Paul G. Fournier and William C. Sleeman, Jr.
Langley Research Center

SUMMARY

A low-speed investigation was conducted over an angle-of-attack range from about -4° to 20° in the Langley V/STOL tunnel to determine the static longitudinal and lateral stability characteristics of a general research model which simulated an advanced configuration for a commercial transport airplane. The model had a 42° swept, aspect-ratio-6.78 wing with a supercritical airfoil and a high-lift system which consisted of a leading-edge slat and a double-slotted flap. Slat deflections of 0° (off), 40°, and 50° in combination with flap deflections of 0°, 20°, and 40° represented clean, take-off, and landing configurations, respectively. Effects on the longitudinal and lateral aerodynamic characteristics were determined for two flow-through, simulated-engine nacelles located on the sides of the fuselage near the rear of the model.

The maximum lift coefficient obtained on the complete model with the high-lift system deflected was 2.26. The static longitudinal stability for all the flap and slat conditions investigated was positive for angles of attack up to about 10° where the stability began to decrease abruptly. Static longitudinal instability was indicated for angles of attack above approximately 14° for all configurations investigated. The static lateral stability derivatives obtained for the complete model showed positive directional stability over the test angle-of-attack range; however, the significant losses in directional stability at high angles of attack indicated that directional instability would be expected for angles somewhat greater than 20°. Lateral control tests with a spoiler on the right wing indicated that the partial-span spoiler was effective in producing positive rolling moments and that positive yawing moments accompanied the rolling moments produced by the spoiler.

INTRODUCTION

Recent research, conducted in a continuing effort by the NASA to improve the performance of subsonic vehicles, has shown that the drag rise can be delayed to Mach

*Title, Unclassified.

numbers near unity by the use of supercritical airfoil sections and by careful integration of the wing, engines, and tail surfaces with a properly shaped fuselage. (See ref. 1.) Much research effort has been undertaken at near sonic speeds to develop aerodynamic configurations that could provide realistic focal points for developing the technology applicable to advanced subsonic commercial transports. Research has also been conducted at low speeds to develop high-lift systems for supercritical airfoils that would enable these advanced configurations to have take-off and landing performance equal to or better than subsonic transports (ref. 2).

The present investigation was conducted to obtain an overall assessment of the low-speed, static-stability, and high-lift performance of an advanced transport configuration that used a high-lift system developed in an earlier unpublished investigation. The wing of the present model had 42° sweep of the quarter chord, an aspect ratio of 6.78, and supercritical airfoil sections. It was located in a low position near the bottom of the fuselage. The high-lift system consisted of a partial-span, double-slotted flap which extended from the fuselage side to the 80-percent-wing-semispan station and a leading-edge slat which extended from the outboard edge of the wing root glove (32-percent-wing-semispan station) to the wing tip. Combinations of flap and slat deflections were investigated to represent clean, take-off, and landing configurations. The horizontal tail was located near the tip of the vertical tail, and various stabilizer settings were investigated for each configuration. Effects of fuselage-mounted nacelles, which were located near the rear of the fuselage, were also determined.

The low-speed tests were conducted in the Langley V/STOL tunnel over an angle-of-attack range from approximately -4° to 20°. Static longitudinal and lateral stability characteristics were determined for the complete model and for the model with the tail surfaces removed. Aerodynamic characteristics were also obtained for a range of spoiler deflections up to 75° to determine the lateral-control effectiveness of an upper-surface spoiler located on one wing panel.

SYMBOLS

The static longitudinal and lateral stability data are presented about the stability-axis system. The positive directions of forces, moments, and angles are indicated in figure 1. The model moment reference point was located longitudinally at the quarter chord of the wing mean aerodynamic chord (theoretical wing) and the fuselage center line.

The measurements of this investigation are presented in the International System of Units (SI). Details concerning the use of SI units, together with physical constants and conversion factors, are presented in reference 3.

b wing span, cm

c local chord, cm

c_f chord of flap, cm

c_r wing root chord, cm

c_s chord of leading-edge slat, cm

c_t wing-tip chord, cm

c_{th} theoretical-wing chord, cm

c_v chord of flap vane, cm

$\bar{c}$ mean aerodynamic chord of theoretical wing, cm

$\bar{c}_h$ mean aerodynamic chord of horizontal tail, cm

$\bar{c}_v$ mean aerodynamic chord of vertical tail, cm

c' portion (0.755c) of basic wing ahead of flap vane, cm

C_D drag coefficient, $\frac{\text{Drag}}{qS}$

C_L lift coefficient, $\frac{\text{Lift}}{qS}$

$C_{L,max}$ maximum value of C_L

$C_{L,trim}$ lift coefficient for longitudinal trimmed condition $(C_m = 0)$

C_l rolling-moment coefficient, $\frac{\text{Rolling moment}}{qSb}$

C_m pitching-moment coefficient, $\frac{\text{Pitching moment}}{qS\bar{c}}$

C_n yawing-moment coefficient, $\frac{\text{Yawing moment}}{qSb}$

C_Y side-force coefficient, $\frac{\text{Side force}}{qS}$

C_{l_β} effective-dihedral parameter, $\frac{\Delta C_l}{\Delta\beta}$, per deg

C_{n_β} directional-stability parameter, $\frac{\Delta C_n}{\Delta\beta}$, per deg

C_{Y_β} side-force parameter, $\frac{\Delta C_Y}{\Delta\beta}$, per deg

i_t incidence of horizontal tail, positive when trailing edge is down (see fig. 1), deg

$i_{t,trim}$ horizontal-tail incidence for longitudinal trimmed condition $(C_m = 0)$, deg

l_t tail length (distance from moment reference $(\bar{c}/4)$ to $(\bar{c}_h/4)$), cm

q free-stream dynamic pressure, N/m^2

R_{le} wing-airfoil-section leading-edge radius, cm

S wing area (based on theoretical planform, glove not included), m^2

t_{max} airfoil-section maximum thickness, cm

t_{te} airfoil-trailing-edge thickness, cm

x distance along chord of selected wing, slat, or flap element (see tables and fig. 2(c)), cm

Δx_{le} distance from leading edge of glove to leading edge of theoretical planform at a given spanwise station, cm

y spanwise distance measured from fuselage center line, cm

z_l lower ordinate of airfoil section, cm

z_u upper ordinate of airfoil section, cm

z_{le} vertical distance from reference line to chord line at leading edge, cm

z_{te} vertical distance from reference line to chord line at trailing edge, cm

α angle of attack of wing reference line, deg

β angle of sideslip, deg

δ_f flap deflection angle with respect to wing chord line, deg

δ_s leading-edge slat deflection angle with respect to wing chord line, deg

$\delta_{spoiler}$ wing upper-surface spoiler deflection relative to wing surface, deg

δ_v vane deflection of double-slotted flap with respect to wing chord line, deg

Λ sweepback angle, measured at quarter-chord line, deg

ϕ wing twist, positive when trailing edge is down, deg

ϵ effective downwash angle, deg

Model components:

W wing

F fuselage

V vertical tail

H horizontal tail

N nacelles

MODEL DESCRIPTION

The model used in the present investigation was a general research model that was modified to simulate an advanced transport configuration by the addition of a large glove over the inboard part of the wing, flow-through nacelles mounted on the rear of the fuselage, and a T-tail. A drawing of the complete model is presented in figure 2(a). Details

of the wing, glove, and high-lift system are shown in figures 2(b) and 2(c), and the upper-surface spoiler that was installed on only the right wing is shown in figure 2(d). Photographs of the model are presented in figure 3.

Wing

The basic wing planform had supercritical airfoil sections, 42° sweep of the quarter-chord line, an aspect ratio of 6.78, and a taper ratio of 0.36. The basic aluminum wing was fitted with a fiber-glass glove over the inboard part which resulted in the planform shown in figure 2(a) and table I. This planform is an approximation of the supercritical wing used on an NASA experimental flight test airplane. The chord, twist, and maximum-thickness variation with span for the glove and wing are shown in figure 2(b) and detailed coordinates of the wing are presented in table I. The basic geometric characteristics are summarized in table II. The wing had a negative dihedral angle of 1.71°. Transition strips, 0.32 cm wide, of No. 80 carborundum were applied to the upper and lower surfaces of the wing 3.81 cm behind the leading edge.

High-Lift System

The high-lift system of the model consisted of a partial-span, double-slotted flap which extended from the wing-body juncture to the 80-percent-wing-semispan station and a slat which extended from the outboard edge of the glove (32-percent-wing-semispan station) to the wing tip. The chord of the double-slotted flap was taken as the aft 35 percent of the basic supercritical airfoil, except at the trailing edge of the inboard portion where the glove was located. The leading edge of the flap was rounded to the nose contour of a modified NACA 4415 airfoil in order to nest within the basic airfoil from 0.650c to 0.755c and to allow 0.159 cm for the upper-surface thickness of the airfoil at 0.755c. The chord of both the vane and the leading-edge slat was 15 percent of the basic wing chord. Both of these elements had St. Cyr 156 airfoil sections modified in thickness ratio at the inboard end and at the tip as shown by the coordinates in tables III and IV.

The geometry of the flap, vane, and slat was defined in a reference deflection position of 50° for the flap and 40° for the slat. The coordinates for the full-span double-slotted flap (although tested herein as a partial-span double-slotted flap) are presented in table V, and the coordinates for the leading-edge slat are presented for several spanwise stations parallel to the plane of symmetry in table III. The flap-vane coordinates are presented in table IV. The angle between the vane and flap was fixed at 25°. Deflections of the flap-vane combination and the leading-edge slat were measured in the streamwise plane (fig. 2(c)) relative to their respective reference chord lines. Transition strips, 0.32 cm wide, of No. 60 carborundum were applied to the upper and lower surfaces of the leading-edge slat 2.54 cm behind the leading edge of the slat.

Spoiler

A spoiler was attached to the upper surface of the right wing to investigate its effectiveness as a roll-control device. The spoiler was made of 0.159-cm-thick metal and was located along the 60-percent-chord line from 32 to 80 percent of the wing semispan (fig. 2(d)). Deflection angles of 4°, 8°, 15°, 30°, 60°, and 75°, with respect to the wing surface along the 60-percent-chord line, were investigated. Part of the wing immediately behind the spoiler was removed when the high-lift system was deflected in order to provide the gap between the wing and flap vane that would normally occur on an aircraft equipped with this type of spoiler.

Fuselage

The fuselage of the model had a modified cylindrical cross section, with circular bottom and top portions and flat sides. Overall dimensions of the fuselage are shown in figure 2(a). A fiber-glass-resin shell, 0.32 cm thick, formed the outer shape of the fuselage and was attached to a metal strongback which housed the six-component strain-gage balance. An electronic angle-of-attack sensor was mounted to the internal strongback to provide the measured geometric angle of attack of the model during the tests.

Tail Surfaces

The location and principal dimensions of the horizontal and vertical tails are given in figure 2(a) and table II. Both tail surfaces were made of aluminum. They had 45° swept leading edges and flat-plate airfoil sections with a rounded leading edge. The vertical tail was 2.54 cm thick and the horizontal tail was 1.27 cm thick. The horizontal tail was attached near the tip of the vertical tail by angle brackets which were drilled to provide a range of incidence angles from 5° to -15°.

Nacelles

Twin fuselage-mounted nacelles were located on the sides of the fuselage near the rear (fig. 2(a)) in order to determine if there were significant aerodynamic effects for such an engine arrangement at low speeds and with the high-lift system deflected. The nacelles were constructed of wood and were attached to the internal strongback through the stub pylons. Constant-internal-diameter openings provided straight flow-through nacelles.

TESTS AND CORRECTIONS

The investigation was conducted in the Langley V/STOL tunnel; most of the tests were run at a dynamic pressure of 2394 newtons/meter^2. The test Reynolds number at

this dynamic pressure was 2.47×10^6 based on the wing mean aerodynamic chord of 0.579 meter. The test dynamic pressure had to be reduced to about one-half of the generally used value in the tests with high spoiler deflections and high-lift system deflections in order to prevent overloads on the strain-gage balance.

Longitudinal aerodynamic characteristics were obtained from tests conducted through an angle-of-attack range from approximately -4° to 20° in increments of 2°. Various stabilizer incidences were investigated to define the trimmed characteristics over the test angle-of-attack range and to obtain effective downwash angles. Tests were also made with the horizontal tail removed to define the tail-off aerodynamic characteristics.

Lateral stability derivatives were obtained from tests conducted through the angle-of-attack range with the model at sideslip angles $\pm 5^\circ$. Lateral stability tests were conducted with the horizontal tail, vertical tail, and nacelles removed in order to determine the contribution of these components.

Aerodynamic characteristics were determined for the clean configuration with the flaps undeflected and the leading-edge slat removed. A take-off configuration was represented by 20° flap deflection and 40° deflection of the leading-edge slat; a landing configuration was represented by 40° flap deflection and 50° deflection of the slat.

Jet-boundary corrections, determined from reference 4, and blockage corrections, obtained from reference 5, were applied to the measured data. The drag data were corrected for balance chamber pressure at the fuselage but were not corrected for effects of the flow through the nacelles. The small differences in drag obtained with and without the nacelles suggest that the drag increment associated with flow through the nacelles was negligible.

PRESENTATION OF RESULTS

The longitudinal and lateral aerodynamic characteristics obtained on the present model for the various test conditions and model configurations are presented in the figures as follows:

DISCUSSION

Longitudinal Characteristics

Effect of nacelles.- Longitudinal stability characteristics were obtained with and without the fuselage-mounted nacelles installed for all flap-slat conditions investigated. Effects of the nacelles on the longitudinal forces and moments were found to be relatively small in the present low-speed tests. (See figs. 4 and 5, for example.) Therefore, they had little influence on the overall low-speed aerodynamic characteristics of the model.

Lift performance.- The lift performance obtained for the model without the nacelles may be summarized as follows:

Configuration	δ_s, deg	δ_f, deg	$C_{L,max}$ ($i_t = 5^o$)	$C_{L,trim}$ at –		
				$\alpha = 0^o$	$\alpha = 5^o$	$\alpha = 20^o$
Clean	Off	0	1.38	0.15	0.54	1.35
Take-off	40	20	2.18	.68	1.11	2.00
Landing	50	40	2.26	1.12	1.50	2.05

Values given as maximum lift coefficients may not actually represent the maximum attainable lift because the test angle of attack was limited to 20^o; the reduction in lift that normally accompanies wing stall was not indicated for the 0^o and 20^o flap deflections. Trimmed lift coefficients at angles of attack below the angle for maximum lift are, however, of more interest because the maximum usable operational lift coefficient must be lower than the maximum lift to provide the margins required for flight safety in commercial transport operation.

The increment in trimmed lift coefficients that resulted from deflection of the high-lift system at 0^o angle of attack was about 0.53 for the take-off configuration ($\delta_s = 40^o$, $\delta_f = 20^o$) and 0.97 for the landing configuration ($\delta_s = 50^o$, $\delta_f = 40^o$). The lift increment obtained for the take-off configuration increased as the angle of attack increased, whereas the incremental lift for the landing configuration decreased as the angle of attack was increased from 0^o. (See fig. 20.) At the highest test angle of attack, the trimmed lift for both the take-off and landing configurations was about the same. The loss in lift effectiveness of the high-lift system at the high deflection angles and high angles of attack occurred primarily because of the direct effects of separated flow on the wing at the high flap deflections rather than from an indirect effect due to trimming. (Compare lift data from figs. 7 and 9.)

Longitudinal stability.- The pitching-moment data presented in figures 4 to 9 indicate that the longitudinal stability for all flap conditions investigated was positive for angles of attack up to about 10^o, but longitudinal instability was indicated for angles of attack above about 14^o. This instability at high angles of attack is also shown for trimmed conditions by the reversal in slope of the stabilizer setting for trim presented in figure 20.

The longitudinal instability at high angles of attack ($C_{L,trim}$ above 1.0) for the clean configuration was particularly severe. (See figs. 4, 5, and 20.) This large instability can be attributed primarily to the large destabilizing increase in the downwash gradient ($\partial\epsilon/\partial\alpha$) shown in figures 18(b) and 19(b). Increasing instability of the wing-body

configuration as the angle of attack increased also contributed to the instability of the complete model in the clean configuration. The stabilizer effectiveness parameter $\left(\partial C_m/\partial i_t\right)$ for all configurations investigated was approximately -0.0450 per degree over the tail angle-of-attack range of the expected linear portion of the tail lift curve. The horizontal-tail effectiveness showed no appreciable decreases throughout the model angle-of-attack range (except where the tail appeared to be stalled at low α and large negative i_t values). Therefore, the loss of stability at high angles of attack for any of the model configurations investigated could not be attributed to immersion of the horizontal tail in a low-velocity wake for the angle-of-attack range covered in these low-speed tests.

The longitudinal instability encountered at high angles of attack for the model configurations with the high-lift system deflected (figs. 6 to 9 and 20) can be attributed to both a moderate increase in $\partial\epsilon/\partial\alpha$ at high angles of attack (figs. 18(b) and 19(b)) and to increasing instability of the tail-off configurations.

Lateral Stability Characteristics

Directional stability.- The static lateral stability derivatives presented in figures 13 to 17 showed positive values of the static directional-stability parameter $\left(C_{n_\beta}\right)$ for the complete model throughout the angle-of-attack range investigated. The static directional stability for all flap deflections showed significant losses in C_{n_β} at high angles of attack; the data trends indicate that directional instability for the complete model would be expected to occur for angles of attack somewhat greater than 20°.

Effective dihedral.- In general, negative values of the effective-dihedral parameter $\left(C_{l_\beta}\right)$ were obtained for positive lift conditions (figs. 13 to 17). Deflection of the high-lift system caused large increases in effective dihedral $\left(-C_{l_\beta}\right)$ at moderate and high angles of attack. (See figs. 13, 15, and 17.) No large, abrupt losses or reversals in the effective dihedral were indicated throughout the test angle-of-attack range, although moderate losses were shown for the clean configuration near 15° angle of attack (figs. 13 and 14).

Vertical-tail contribution.- Test results obtained with the vertical tail on and off (figs. 13, 15, 16, and 17) showed significant reductions in the tail contribution to static directional stability as the model angle of attack was increased. The powerful end-plate effect of the horizontal tail on the vertical tail is shown by the derivatives presented in figures 13 and 15. The end-plate effect of the horizontal tail provided an increment of directional stability that was almost invariant with angle of attack, whereas the contribution of the vertical tail alone to C_{n_β} generally decreased at the high angles of attack.

The end-plate effect, shown in the side-force parameter $\left(C_{Y_\beta}\right)$ for the clean configuration (fig. 13), shows a considerable decrease in the effect of the horizontal tail at the highest angles of attack. This loss in end-plate effect on C_{Y_β} suggests that the presence of the horizontal tail shifted the center of pressure on the vertical tail rearward and, thereby, maintained nearly constant end-plate effect on C_{n_β} at high angles of attack.

Effect of nacelles.- Addition of the fuselage-mounted nacelles generally had small overall effect on the measured lateral stability derivatives. The only appreciable effect of the nacelles on the lateral stability derivatives was a small increase in directional stability at high angles of attack for the landing configuration (fig. 17).

Lateral Control

The use of a partial-span spoiler for lateral control was investigated with a flap-type spoiler located on the upper surface of the right wing. Part of the wing immediately behind the spoiler was removed when the high-lift system was deflected to provide the gap between the wing and flap vane that would normally occur on an aircraft equipped with this type of spoiler (fig. 2(d)). Spoiler deflection angles ranging up to 75° were investigated for the clean, take-off, and landing configurations, and the results are presented in figures 10 to 12.

Deflection of the spoiler decreased the lift, increased the drag, and caused a positive increment in pitching moment; it also provided the desired rolling moment. Positive yawing moments and negative side forces accompanied the positive rolling moments produced by the spoiler. The magnitude of these incremental effects increased with deflection of the high-lift system. Almost complete loss of rolling effectiveness occurred for the clean configuration at the highest test angles of attack, probably because flow separation was well developed on the outboard portion of the plain wing without the spoiler. Effectiveness of the spoiler at high angles of attack with the high-lift system deflected remained high because the leading-edge slat had a large beneficial effect on the flow separation; the wing with the slat deflected was carrying a large amount of lift that could be spoiled by deflection of the spoiler.

SUMMARY OF RESULTS

A low-speed investigation was conducted in the Langley V/STOL tunnel to determine the static longitudinal and lateral stability characteristics of a general research model that simulated an advanced transport airplane. The model had an aspect-ratio-6.78, 42° swept wing with a supercritical airfoil and a high-lift system which consisted of a

leading-edge slat and a double-slotted flap. The results of this investigation may be summarized as follows:

1. The maximum lift coefficient obtained for the clean configuration was 1.38. Deflection of the high-lift system for a landing condition (slat at 50°, flap at 40°) increased the maximum lift coefficient of 2.26. Deflection of the horizontal tail to provide trim for the landing configuration reduced the maximum lift coefficient at 20° to 2.05.

2. The static longitudinal stability for all the flap and slat conditions investigated was positive for angles of attack up to about 10° where the stability began to decrease abruptly. Longitudinal instability was indicated for angles of attack above approximately 14°.

3. Static lateral stability derivatives obtained for the complete model showed positive directional stability throughout the test angle-of-attack range. However, significant decreases in directional stability occurred at high angles of attack, and directional instability would be expected to occur for angles of attack somewhat greater than 20°. Negative values of the effective-dihedral parameter were obtained for positive lift conditions, and deflection of the high-lift system caused large increases in effective dihedral at moderate and high angles of attack.

4. Lateral-control tests indicated that a partial-span spoiler on the right wing was effective in producing positive rolling moments over a deflection range to 75°. Positive yawing moments and negative side forces accompanied the positive rolling moments produced by the spoiler. Almost complete loss of effectiveness occurred for the clean configuration at high angles of attack. However, with the high-lift system deflected, the effectiveness of the spoiler remained high because of the beneficial effect of the leading-edge slat at high angles of attack.

Langley Research Center,
National Aeronautics and Space Administration,
Hampton, Va., July 31, 1972.

REFERENCES

1. Langhans, Richard A.; and Flechner, Stuart G.: Wind-Tunnel Investigation at Mach Numbers From 0.25 to 1.01 of a Transport Configuration Designed to Cruise at Near-Sonic Speeds. NASA TM X-2622, 1972.

2. Goodson, Kenneth W.: Low-Speed Aerodynamic Characteristics of a Rectangular, Aspect-Ratio-6, Slotted Supercritical Airfoil Wing Having Several High-Lift Flap Systems. NASA TM X-2317, 1971.

3. Mechtly, E. A.: The International System of Units – Physical Constants and Conversion Factors (Revised). NASA SP-7012, 1969.

4. Gillis, Clarence L.; Polhamus, Edward C.; and Gray, Joseph L., Jr.: Charts for Determining Jet-Boundary Corrections for Complete Models in 7- by 10-Foot Closed Rectangular Wind Tunnels. NACA WR L-123, 1945. (Formerly NACA ARR L5G31.)

5. Herriot; John G.: Blockage Corrections for Three-Dimensional-Flow Closed-Throat Wind Tunnels, With Consideration of the Effect of Compressibility. NACA Rep. 995, 1950. (Supersedes NACA RM A7B28.)

TABLE I.- BASIC WING COORDINATES

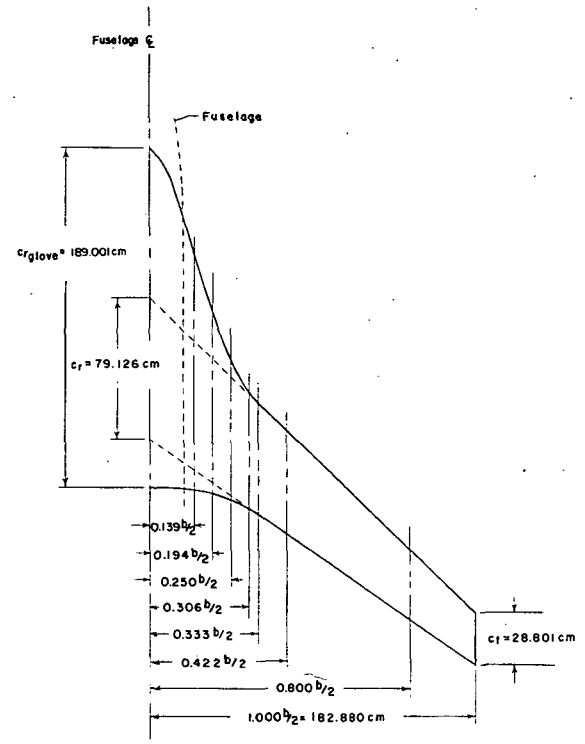

$\frac{y}{b/2}$	0.139		0.194		0.250		0.306		0.333		0.422		0.800		1.000	
c, cm	128.270		99.314		77.724		65.430		62.329		$\bar{c}$ = 57.874		38.867		28.801	
$\frac{x}{c}$	$\frac{z_u}{c}$	$\frac{z_l}{c}$	$\frac{z_u}{c}$	$\frac{z_l}{c}$	$\frac{z_u}{c}$	$\frac{z_l}{c}$	$\frac{z_u}{c}$	$\frac{z_l}{c}$	$\frac{z_u}{c}$	$\frac{z_l}{c}$	$\frac{z_u}{c}$	$\frac{z_l}{c}$	$\frac{z_u}{c}$	$\frac{z_l}{c}$	$\frac{z_u}{c}$	$\frac{z_l}{c}$
0	.0317	.0317	.0281	.0281	.0327	.0327	.0291	.0291	.0294	.0294	.0225	.0225	-.0185	-.0185	-.0635	-.0635
.0025	.0418	.0213	.0432	.0233	.0415	.0235	.0388	.0190	.0367	.0204	.0318	.0132	-.0129	-.0260	-.0595	-.0717
.0050	.0450	.0182	.0471	.0197	.0464	.0186	.0437	.0155	.0408	.0163	.0351	.0103	-.0098	-.0294	-.0573	-.0732
.0100	.0497	.0137	.0531	.0148	.0523	.0144	.0474	.0122	.0448	.0131	.0395	.0073	-.0065	-.0327	-.0539	-.0755
.0200	.0558	.0083	.0596	.0096	.0598	.0092	.0538	.0066	.0490	.0082	.0437	.0033	-.0002	-.0384	-.0502	-.0802
.0300	.0602	.0044	.0639	.0059	.0654	.0057	.0582	.0031	.0530	.0054	.0472	.0000	.0019	-.0414	-.0471	-.0838
.0400	.0636	.0012	.0673	.0031	.0693	.0023	.0609	-.0006	.0557	.0036	.0494	-.0020	.0039	-.0435	-.0441	-.0850
.0500	.0667	-.0012	.0701	.0008	.0719	-.0010	.0631	-.0023	.0579	.0015	.0516	-.0041	.0064	-.0439	-.0440	-.0855
.0750	.0735	-.0065	.0750	-.0041	.0771	-.0049	.0672	-.0066	.0623	-.0020	.0557	-.0075	.0098	-.0441	-.0379	-.0838
.1000	.0778	-.0101	.0788	-.0079	.0794	-.0088	.0695	-.0089	.0660	-.0051	.0595	-.0102	.0146	-.0454	-.0340	-.0836
.1500	.0851	-.0152	.0836	-.0141	.0835	-.0123	.0749	-.0120	.0718	-.0089	.0653	-.0143	.0212	-.0454	-.0264	-.0794
.2000	.0901	-.0190	.0867	-.0179	.0858	-.0141	.0776	-.0144	.0758	-.0108	.0691	-.0154	.0262	-.0438	-.0195	-.0764
.2500	.0923	-.0208	.0885	-.0199	.0876	-.0147	.0804	-.0151	.0775	-.0116	.0724	-.0157	.0325	-.0425	-.0123	-.0713
.3000	.0931	-.0218	.0893	-.0205	.0879	-.0144	.0815	-.0146	.0795	-.0117	.0746	-.0149	.0359	-.0393	-.0066	-.0672
.3500	.0929	-.0220	.0887	-.0192	.0882	-.0137	.0829	-.0136	.0807	-.0105	.0755	-.0140	.0393	-.0370	-.0008	-.0617
.4000	.0917	-.0218	.0872	-.0169	.0873	-.0118	.0823	-.0116	.0811	-.0082	.0762	-.0118	.0432	-.0337	.0052	-.0559
.4500	.0899	-.0200	.0854	-.0143	.0863	-.0092	.0815	-.0093	.0810	-.0061	.0759	-.0096	.0457	-.0306	.0113	-.0508
.5000	.0877	-.0160	.0831	-.0110	.0853	-.0057	.0811	-.0062	.0803	-.0038	.0757	-.0060	.0479	-.0256	.0172	-.0442
.5500	.0842	-.0105	.0806	-.0070	.0833	-.0013	.0800	-.0023	.0795	.0000	.0757	-.0017	.0505	-.0199	.0228	-.0386
.6000	.0807	-.0059	.0780	-.0028	.0807	.0033	.0788	.0027	.0784	.0057	.0755	.0028	.0523	-.0133	.0284	-.0317
.6500	.0758	.0008	.0749	.0026	.0783	.0088	.0776	.0089	.0774	.0133	.0746	.0110	.0545	-.0055	.0340	-.0220
.7000	.0716	.0071	.0739	.0090	.0748	.0144	.0747	.0163	.0761	.0217	.0737	.0204	.0564	.0060	.0381	-.0086
.7500	.0670	.0137	.0668	.0161	.0714	.0219	.0718	.0248	.0741	.0319	.0717	.0300	.0581	.0174	.0425	.0044
.8000	.0626	.0192	.0624	.0226	.0667	.0286	.0681	.0326	.0711	.0408	.0691	.0389	.0575	.0263	.0441	.0150
.8500	.0560	.0253	.0568	.0279	.0614	.0343	.0637	.0388	.0672	.0473	.0658	.0455	.0566	.0344	.0441	.0237
.9000	.0497	.0275	.0504	.0294	.0556	.0373	.0586	.0427	.0622	.0503	.0612	.0483	.0523	.0388	.0439	.0294
.9500	.0418	.0267	.0427	.0281	.0487	.0350	.0524	.0404	.0557	.0412	.0541	.0441	.0458	.0356	.0382	.0289
.9700	.0384	.0255	.0394	.0269	.0458	.0340	.0493	.0384	.0530	.0409	.0509	.0408	.0422	.0326	.0344	.0244
.9800	.0364	.0246	.0381	.0258	.0444	.0327	.0479	.0373	.0511	.0404	.0491	.0384	.0408	.0314	.0301	.0212
.9900	.0347	.0236	.0361	.0253	.0425	.0320	.0462	.0357	.0489	.0376	.0467	.0364	.0388	.0278	.0282	.0184
.9950	.0335	.0232	.0353	.0251	.0422	.0317	.0458	.0349	.0475	.0367	.0455	.0351	.0376	.0262	.0258	.0159
1.0000	.0332	.0226	.0345	.0243	.0415	.0310	.0450	.0344	.0463	.0360	.0444	.0342	.0359	.0250	.0247	.0143
R_{le}/c	.0198		.0210		.0212		.0186		.0155		.0149		.0091		.0031	

TABLE II.- GEOMETRIC CHARACTERISTICS

Wing:	
Area, m^2	1.97
Mean aerodynamic chord, cm	57.87
Span, cm	365.76
Aspect ratio	6.78
Taper ratio	0.36
Dihedral angle, deg	-1.71
Horizontal tail:	
Area, m^2	0.45
Mean aerodynamic chord, cm	40.99
Span, cm	115.67
Aspect ratio	0.75
Taper ratio	0.40
Vertical tail:	
Area, m^2	0.40
Mean aerodynamic chord, cm	68.63
Span, cm	58.85
Aspect ratio	0.87
Taper ratio	0.69

TABLE III.- LEADING-EDGE SLAT COORDINATES

x/c_s	z_u/c_s	z_l/c_s	z_u/c_s	z_l/c_s
	$\frac{y}{b/2} = 0.320$; $c_s = 9.455$ cm		$\frac{y}{b/2} = 1.000$; $c_s = 4.321$ cm	
0	-0.0122	-0.0122	-0.0837	-0.0837
.0125	.0217	-.0351	-.0564	-.1000
.0250	.0366	-.0429	-.0444	-.1041
.0500	.0574	-.0505	-.0270	-.1064
.0750	.0740	-.0538	-.0134	-.1073
.1000	.0887	-.0542	-.0012	-.1061
.1500	.1109	-.0495	.0176	-.0998
.2000	.1277	-.0417	.0326	-.0897
.3000	.1467	-.0238	.0514	-.0682
.4000	.1506	-.0062	.0607	-.0485
.5000	.1461	.0110	.0647	-.0300
.6000	.1320	.0237	.0620	-.0129
.7000	.1076	.0281	.0531	-.0015
.8000	.0776	.0261	.0400	.0031
.9000	.0436	.0170	.0234	.0035
.9500	.0254	.0094	.0138	.0021
1.0000	.0062	0	.0043	0

TABLE IV.- FLAP-VANE COORDINATES

x/c_v	z_u/c_v	z_l/c_v	z_u/c_v	z_l/c_v	z_u/c_v	z_l/c_v
	c_v = 10.795 cm; $\frac{y}{b/2}$ = 0.0139		c_v = 9.455; $\frac{y}{b/2}$ = 0.320		c_v = 4.321 cm; $\frac{y}{b/2}$ = 1.000	
0	-0.0049	-0.0049	-0.0122	-0.0122	-0.0837	-0.0837
.0125	.0300	-.0280	.0217	-.0351	-.0564	-.1000
.0250	.0450	-.0366	.0366	-.0429	-.0444	-.1041
.0500	.0663	-.0446	.0574	-.0505	-.0270	-.1064
.0750	.0832	-.0480	.0740	-.0538	-.0134	-.1073
.1000	.0982	-.0487	.0887	-.0542	-.0012	-.1061
.1500	.1210	-.0442	.1109	-.0495	.0176	-.0998
.2000	.1379	-.0366	.1277	-.0417	.0326	-.0897
.3000	.1547	-.0190	.1467	-.0238	.0514	-.0682
.4000	.1600	-.0016	.1506	-.0062	.0607	-.0485
.5000	.1546	.0150	.1461	.0110	.0647	-.0300
.6000	.1394	.0275	.1320	.0237	.0620	-.0129
.7000	.1135	.0312	.1076	.0281	.0531	-.0015
.8000	.0815	.0295	.0776	.0261	.0400	.0031
.9000	.0457	.0187	.0436	.0170	.0234	.0035
.9500	.0267	.0102	.0254	.0094	.0138	.0021
1.0000	.0065	0	.0062	0	.0043	0

TABLE V.- FLAP COORDINATES

x/c_f	z_u/c_f	z_l/c_f	z_u/c_f	z_l/c_f	z_u/c_f	z_l/c_f
	c_f = 34.392 cm; $\frac{y}{b/2}$ = 0.139		c_f = 22.060 cm; $\frac{y}{b/2}$ = 0.320		c_f = 10.081 cm; $\frac{y}{b/2}$ = 1.000	
0	0.0754	0.0754	0.0903	0.0903	-0.0252	-0.0252
.0100	.1012	.0572	.1184	.0708	-.0016	-.0393
.0200	.1130	.0535	.1296	.0651	.0072	-.0423
.0400	.1307	.0499	.1456	.0596	.0211	-.0452
.0600	.1433	.0499	.1570	.0576	.0317	-.0450
.1000	.1647	.0554	.1741	.0594	.0496	-.0380
.1500	.1824	.0613	.1900	.0669	.0675	-.0244
.2000	.1950	.0679	.1984	.0751	.0821	-.0115
.2500	.2016	.0727	.2030	.0843	.0950	.0006
.3000	.2053	.0790	.2048	.0938	.1046	.0124
.3517	.2072	.0857	.2054	.1035	.1115	.0233
.4189	.2049	.0931	.2030	.1155	.1179	.0373
.4851	.2001	.0982	.1991	.1255	.1228	.0495
.5458	.1950	.1016	.1947	.1336	.1260	.0605
.6160	.1869	.1033	.1890	.1395	.1264	.0706
.6811	.1758	.1033	.1820	.1424	.1256	.0787
.7451	.1669	.1016	.1745	.1414	.1229	.0830
.8089	.1569	.0997	.1668	.1365	.1160	.0816
.8717	.1455	.0975	.1572	.1279	.1061	.0763
.9337	.1352	.0923	.1459	.1166	.0906	.0631
1.0000	.1237	.0842	.1312	.1028	.0691	.0403

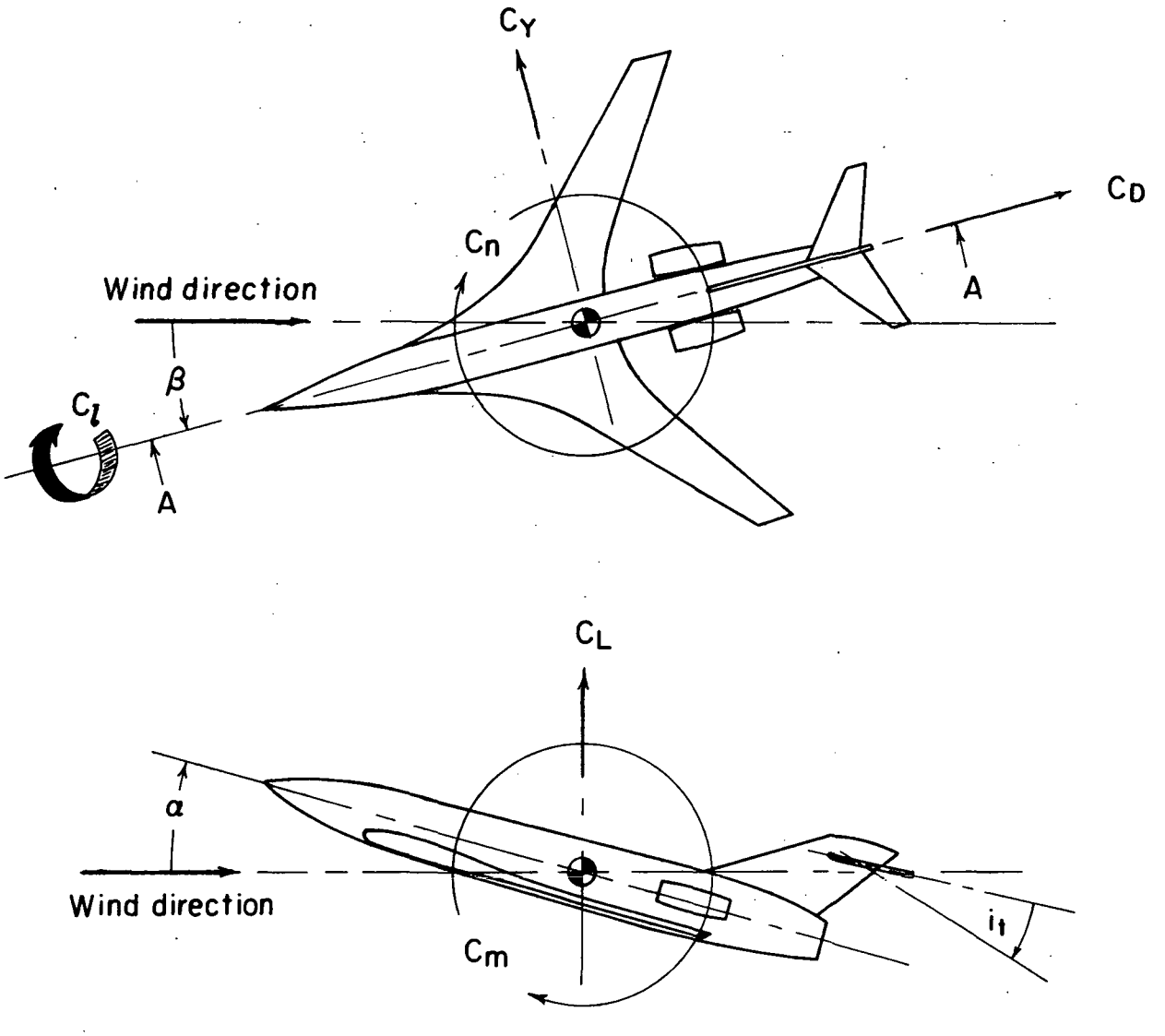

View A-A

Figure 1.- System of axes. Positive directions of forces, moments, and angles are indicated by arrows.

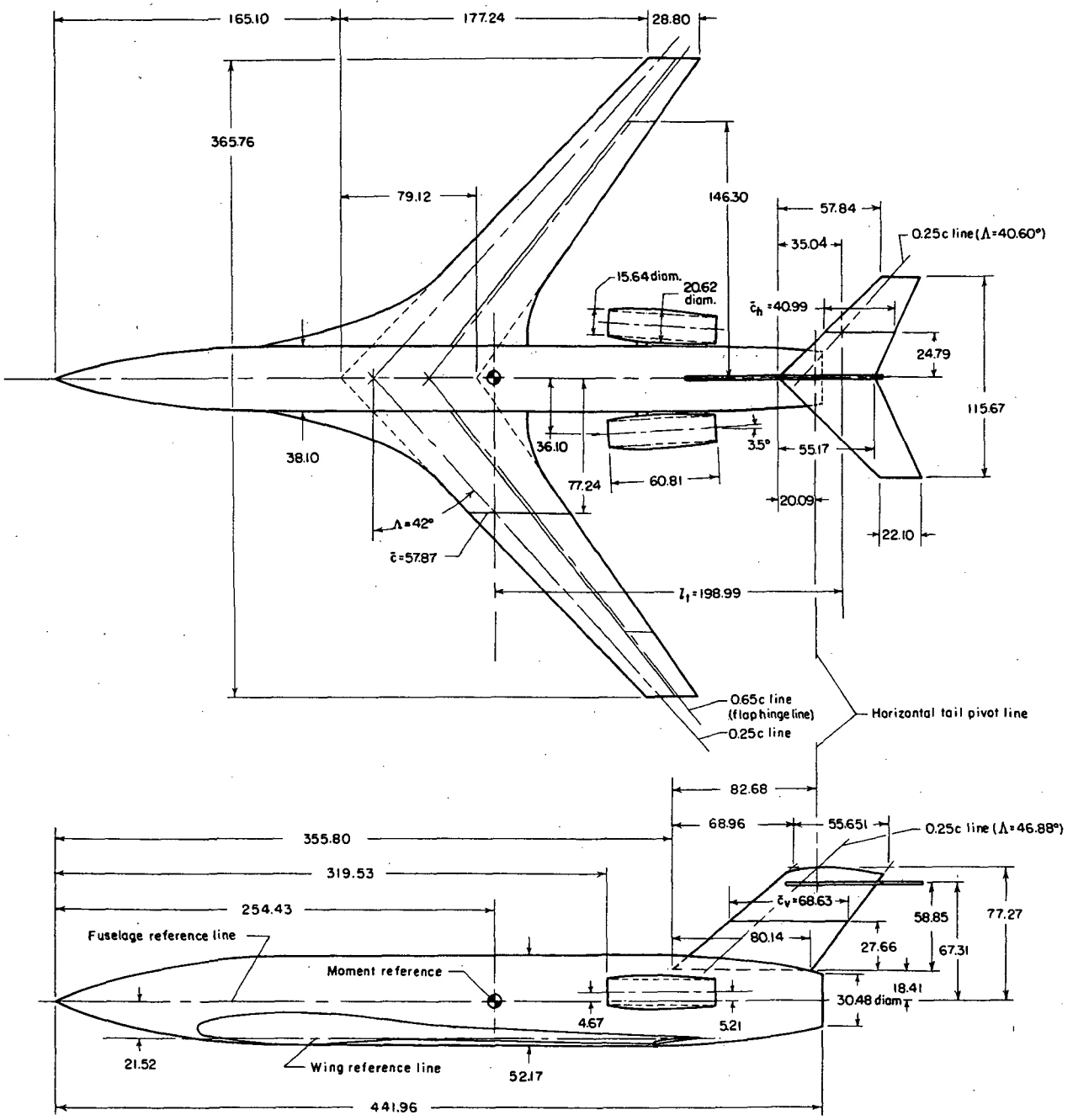

(a) Complete model geometric characteristics.

Figure 2.- Details of model. (Dimensions in centimeters.)

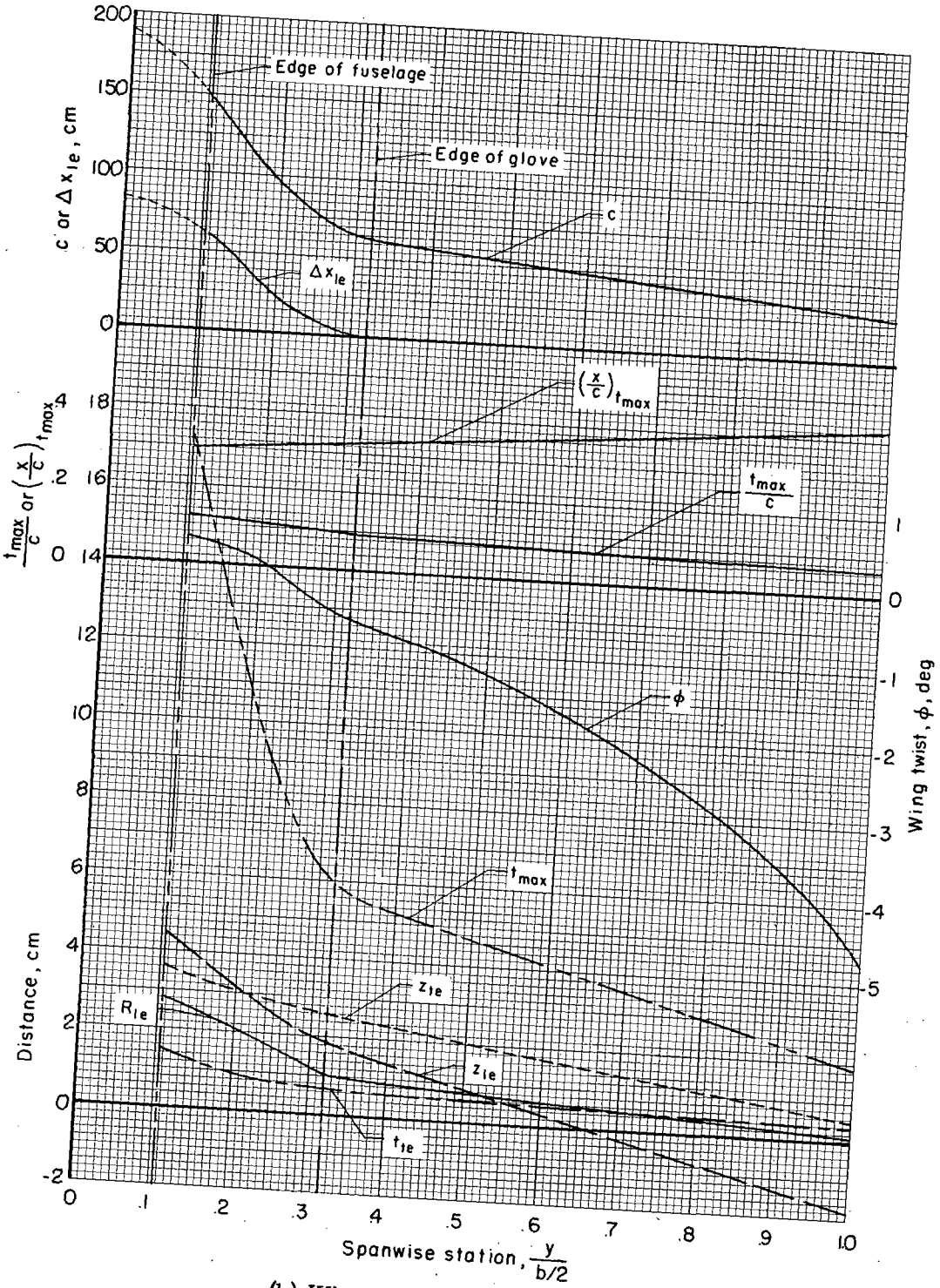

(b) Wing spanwise details.

Figure 2.- Continued.

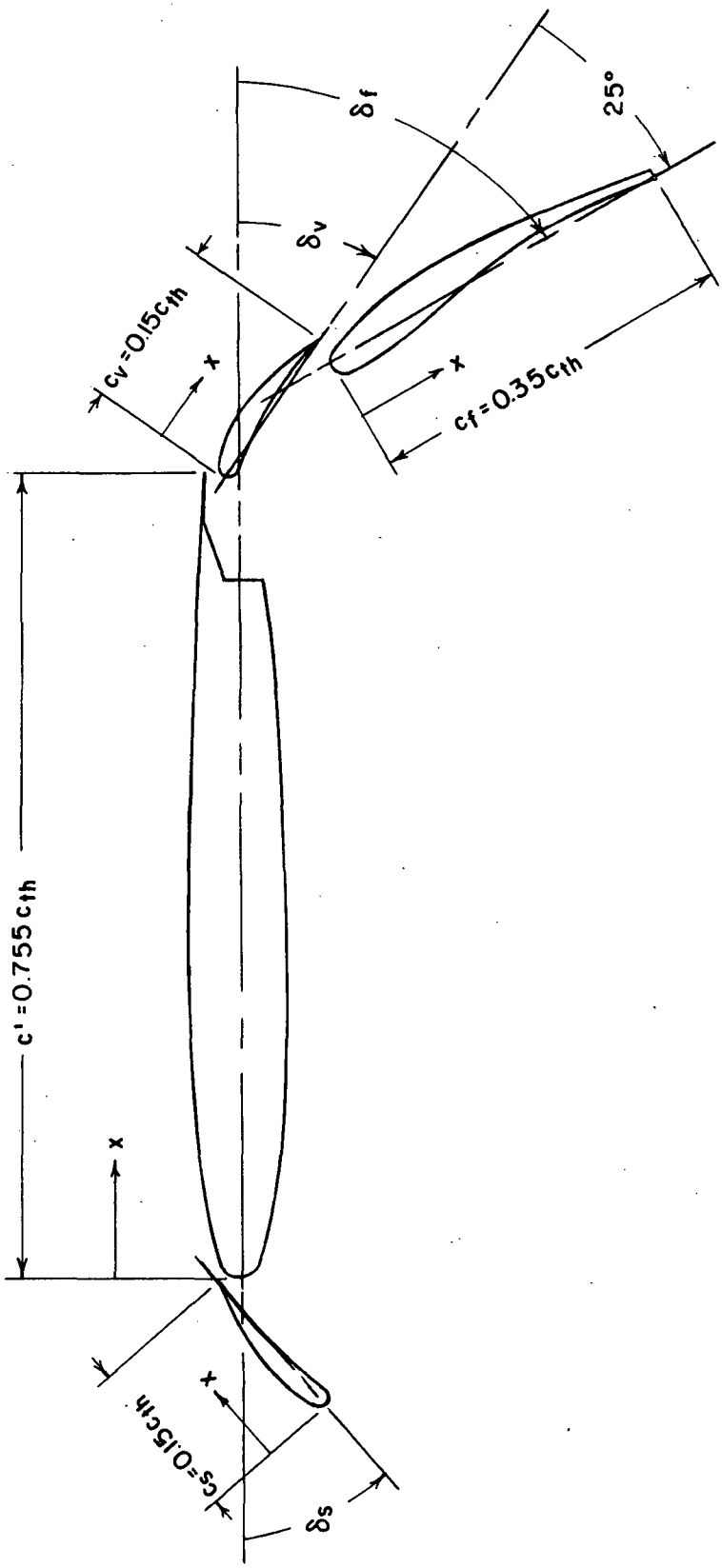

(c) Details of flap and slat system.

Figure 2.- Continued.

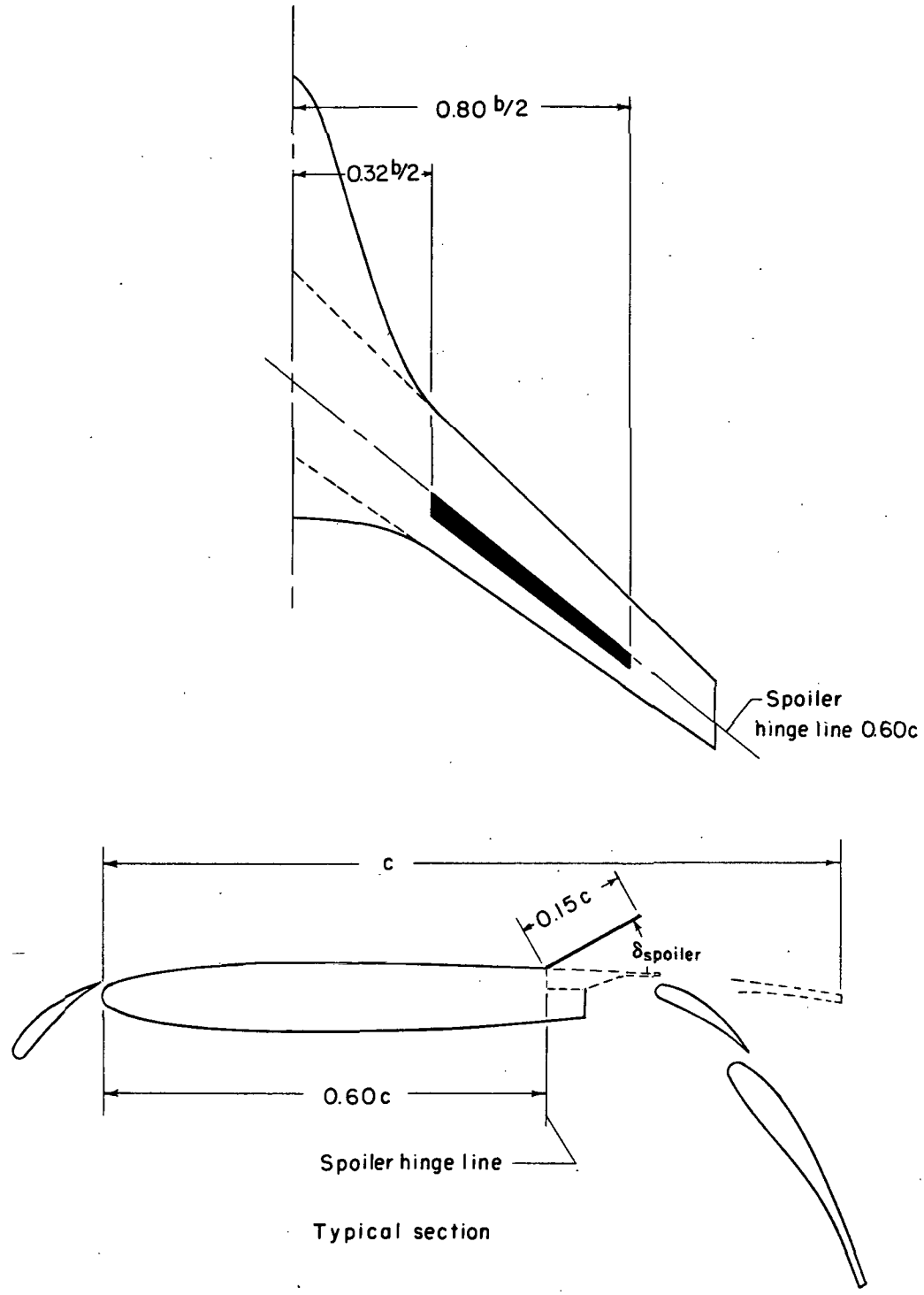

(d) Spoiler description and location.

Figure 2.- Concluded.

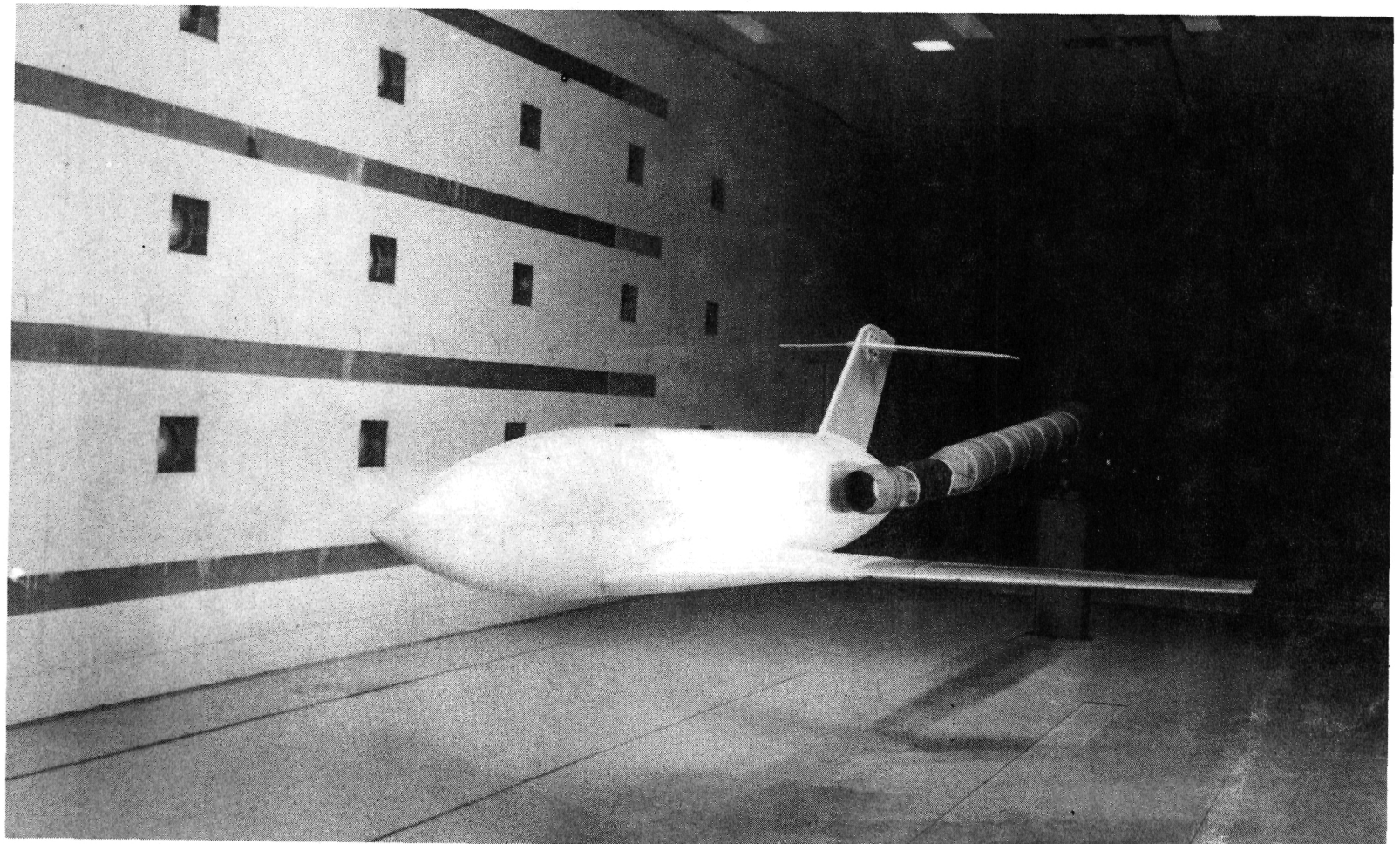

L-71-7559

(a) Clean wing configuration.

Figure 3.- Photographs of complete model in Langley V/STOL tunnel.

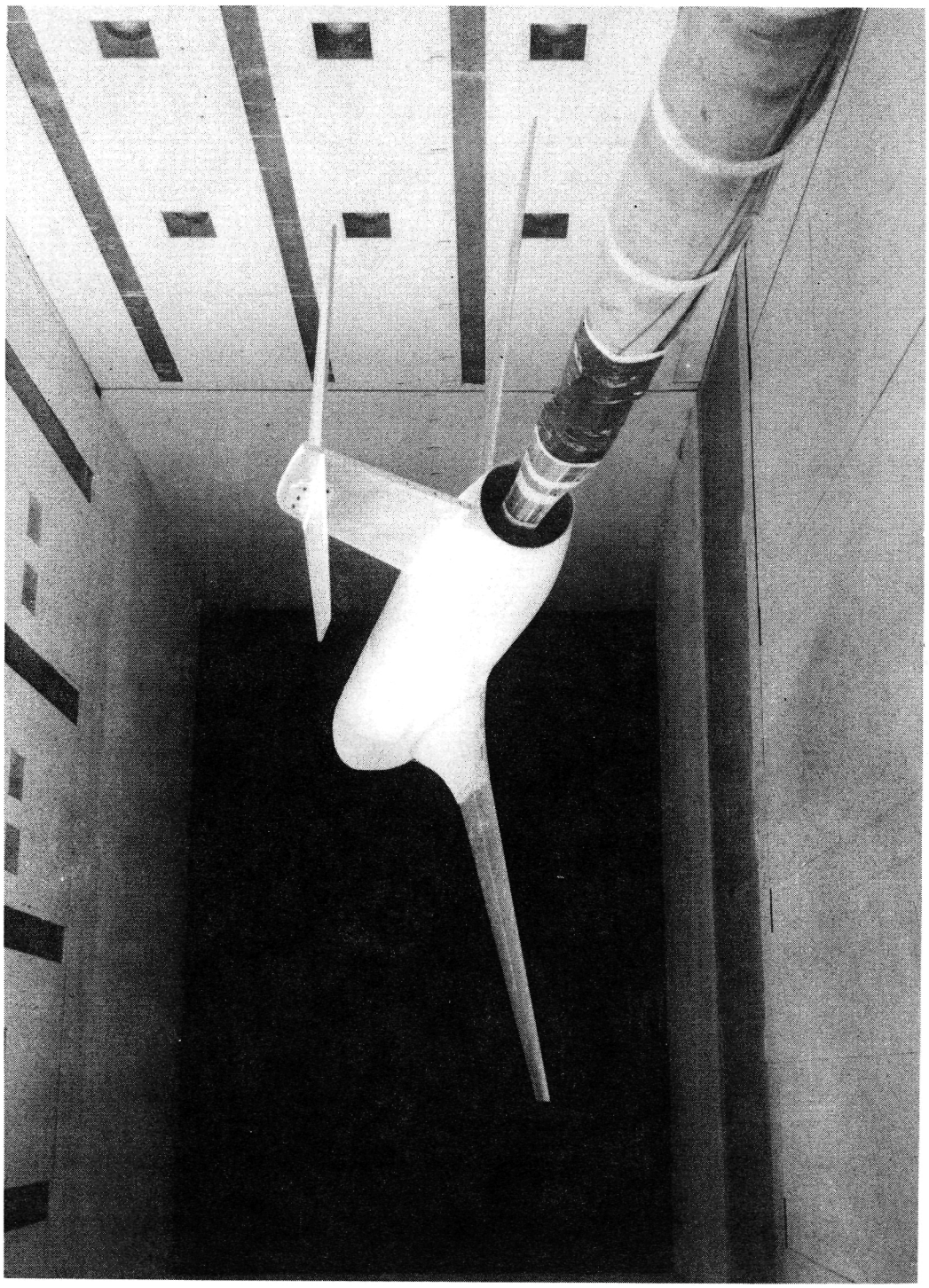

L-71-7554

(a) Concluded.

Figure 3.- Continued.

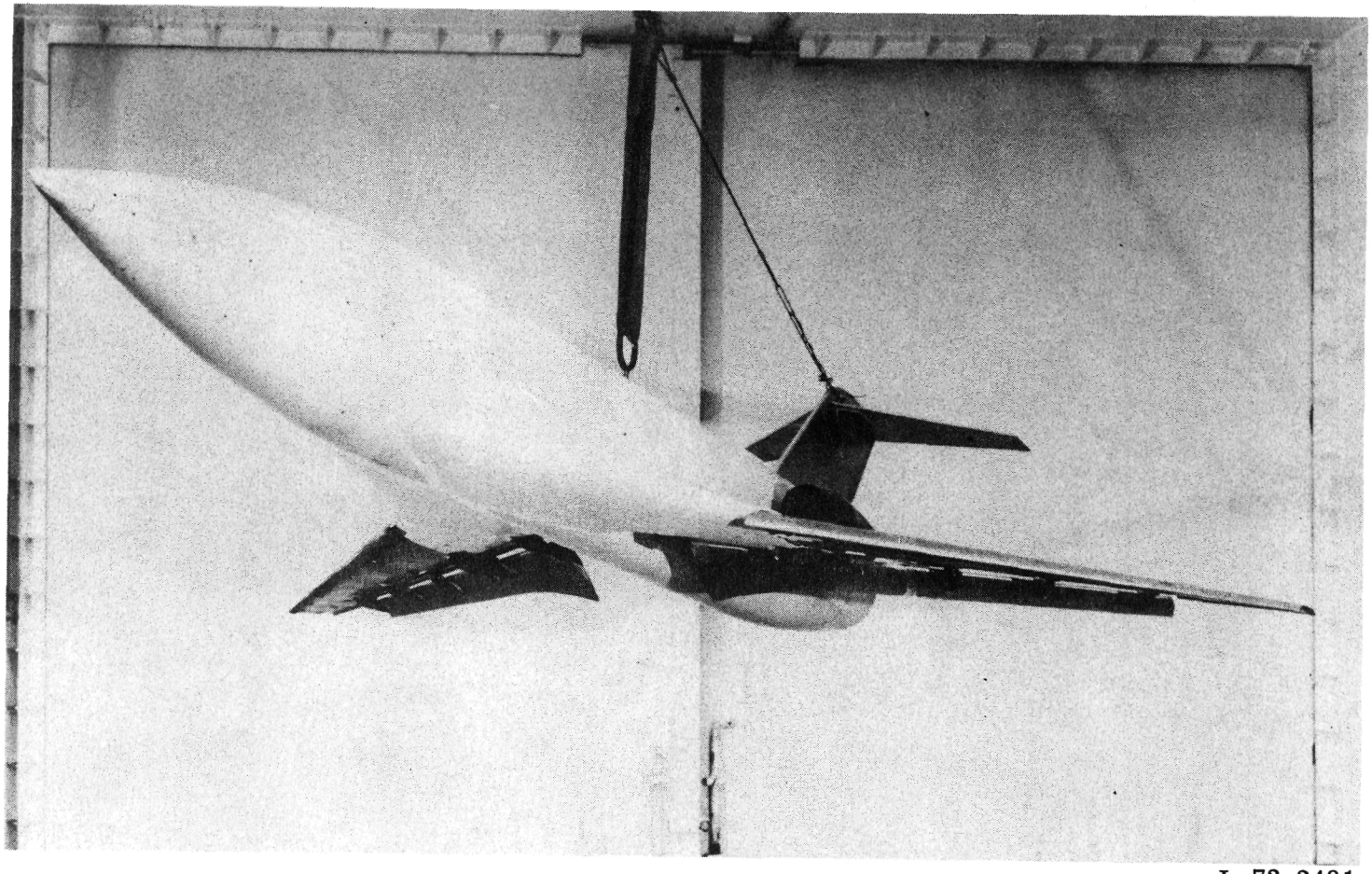

L-72-2481

(b) High-lift system for take-off configuration.

Figure 3.- Continued.

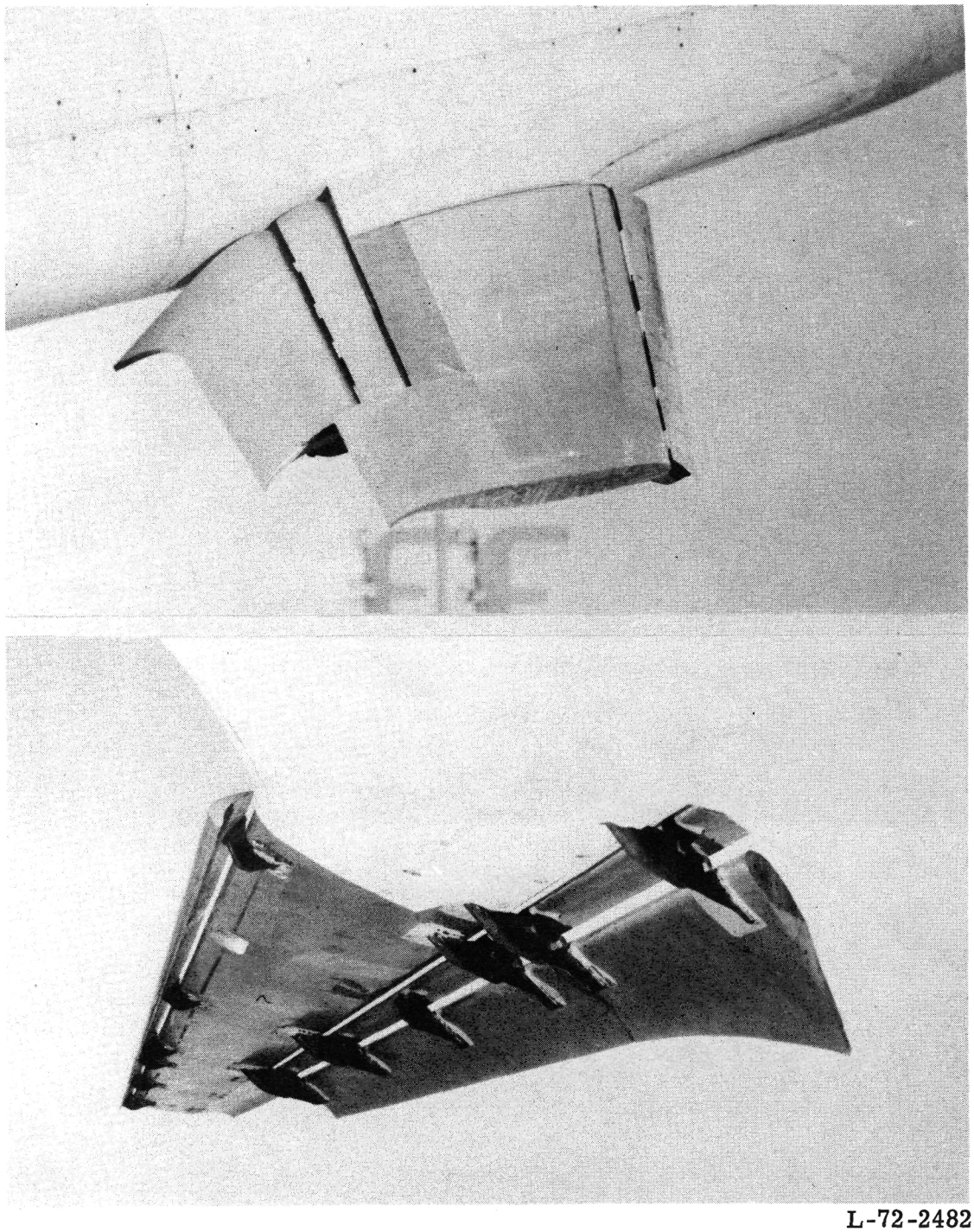

L-72-2482

(b) Concluded.

Figure 3.- Concluded.

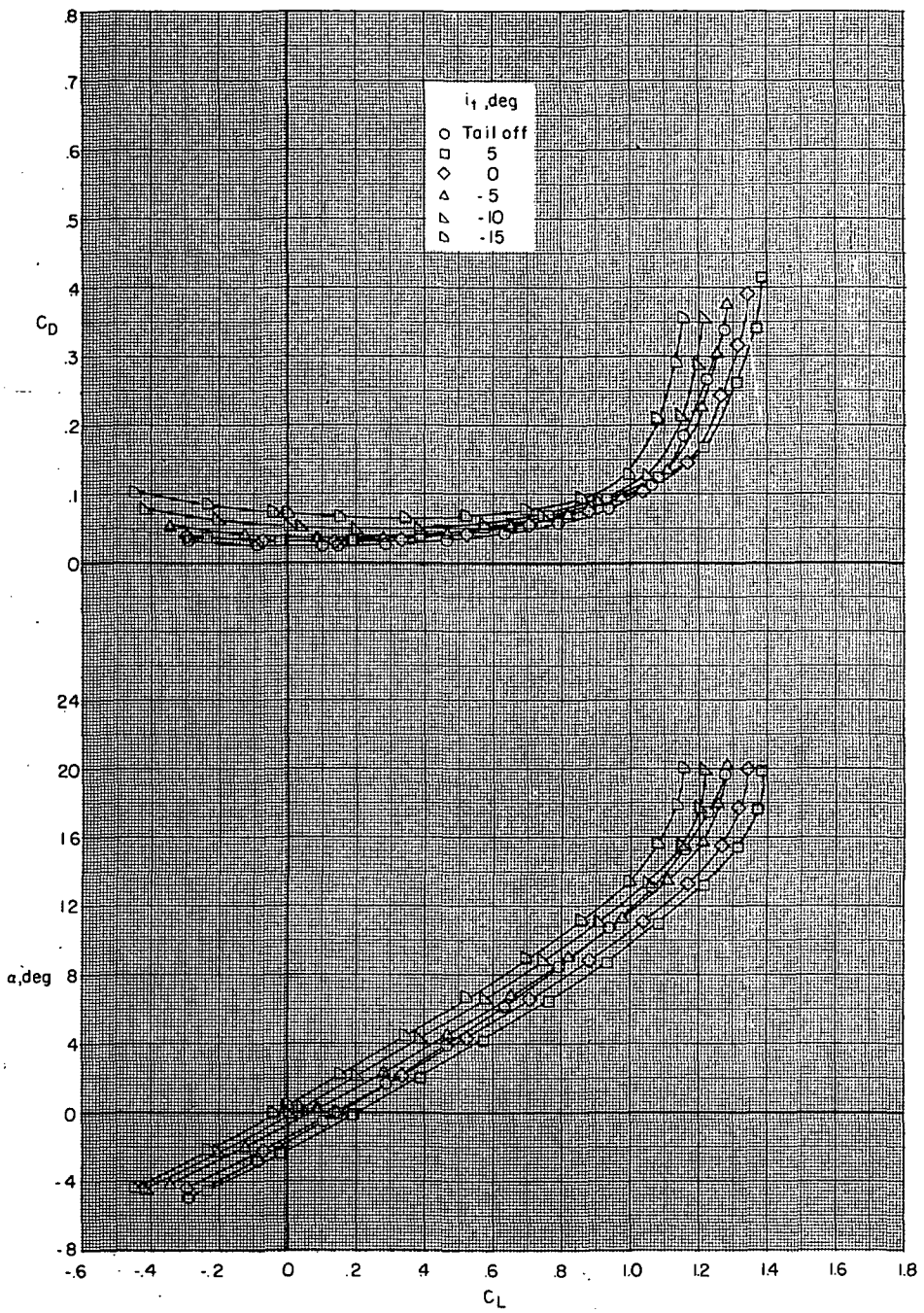

Figure 4.- Effect of horizontal-tail deflection on longitudinal aerodynamic characteristics of clean configuration with nacelles on and slat off; $\delta_f = 0^o$.

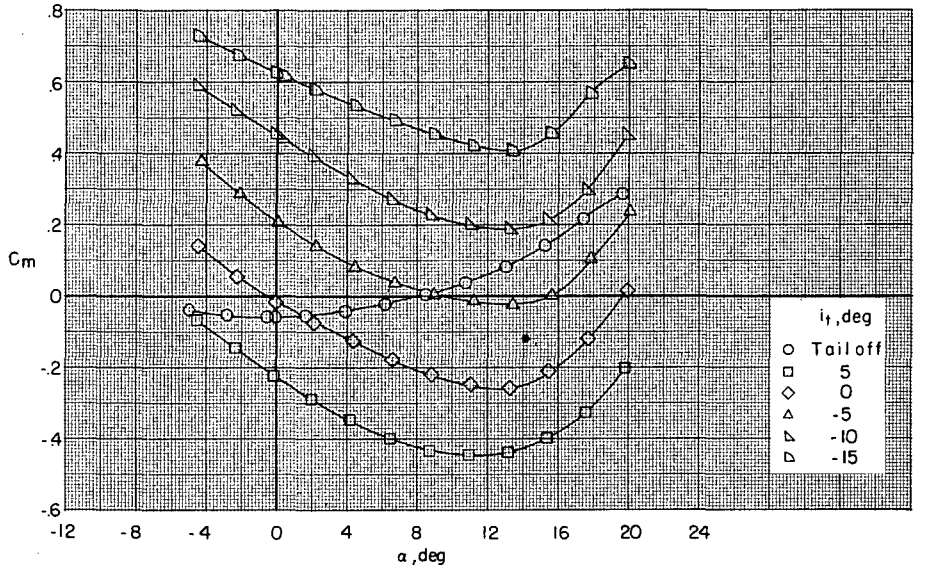

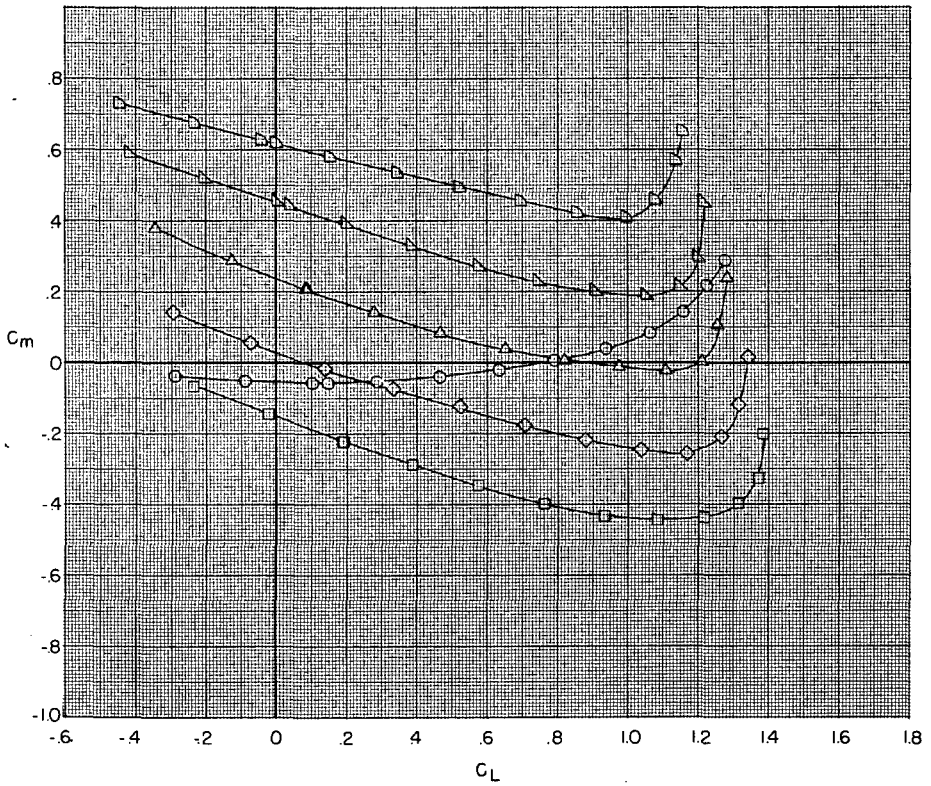

Figure 4.- Concluded.

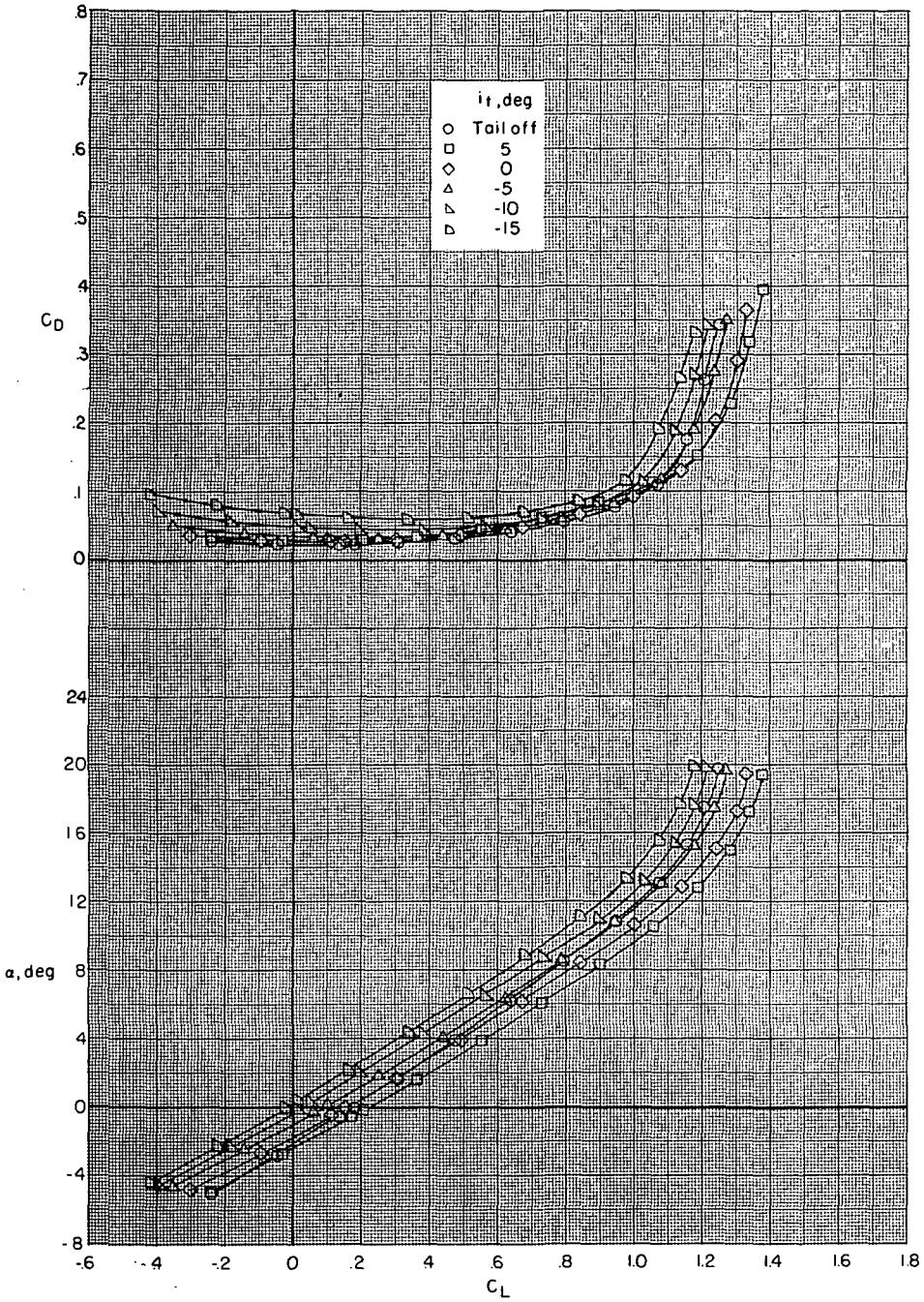

Figure 5.- Effect of horizontal-tail deflection on longitudinal aerodynamic characteristics of clean configuration with nacelles and slat off; $\delta_f = 0^o$.

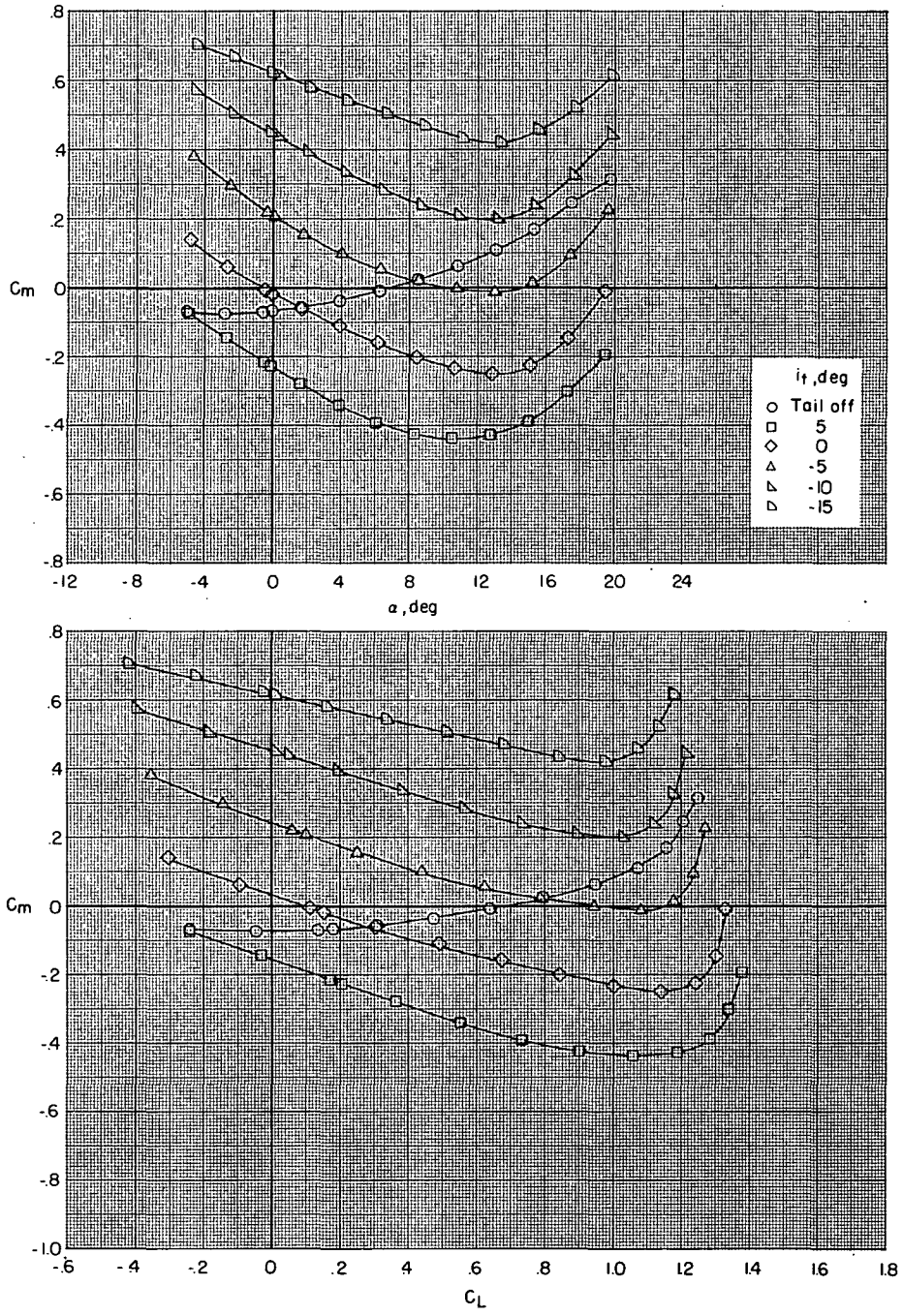

Figure 5.- Concluded.

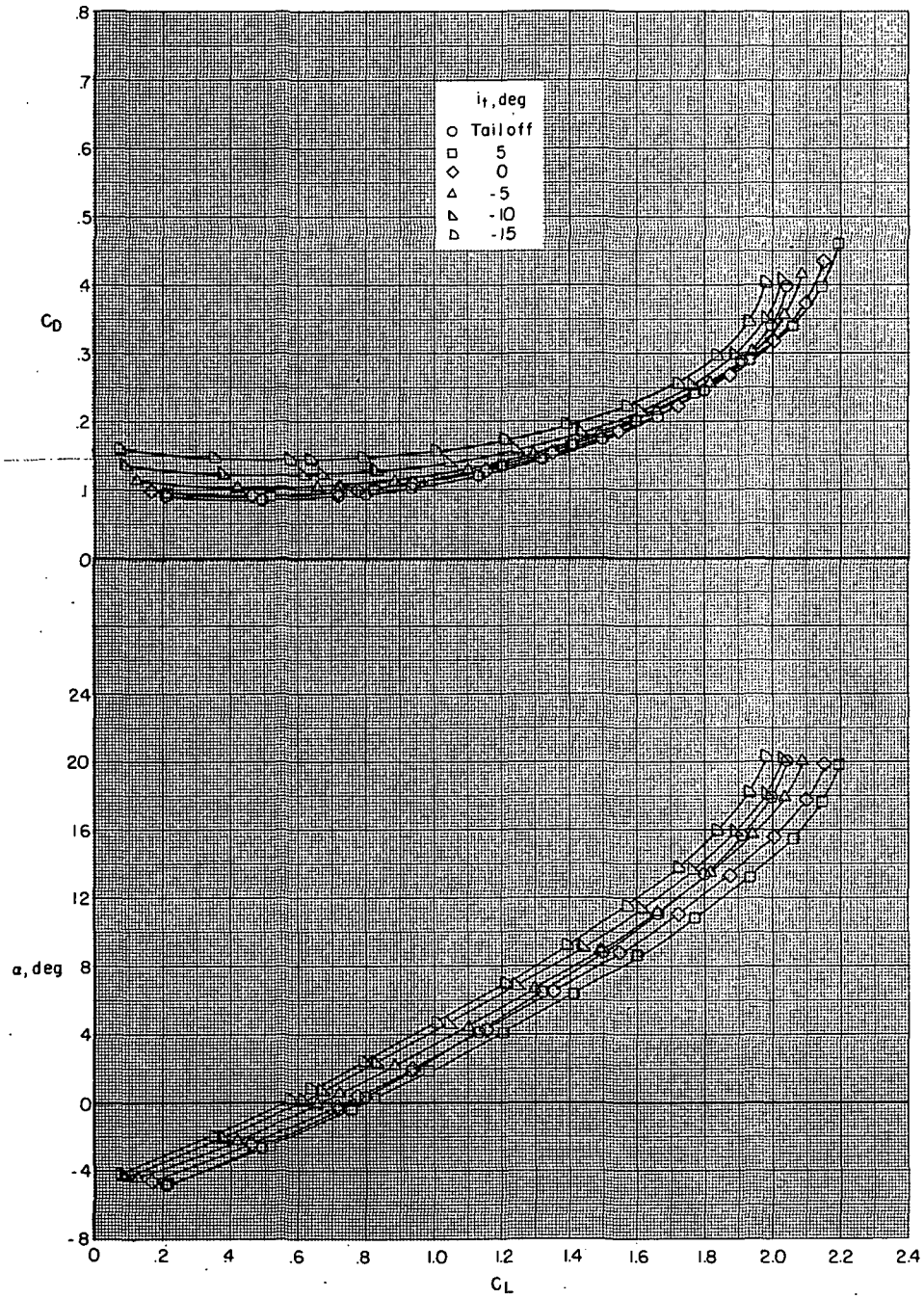

Figure 6.- Effect of horizontal-tail deflection on longitudinal aerodynamic characteristics of take-off configuration with nacelles on. $\delta_s = 40^o$; $\delta_f = 20^o$.

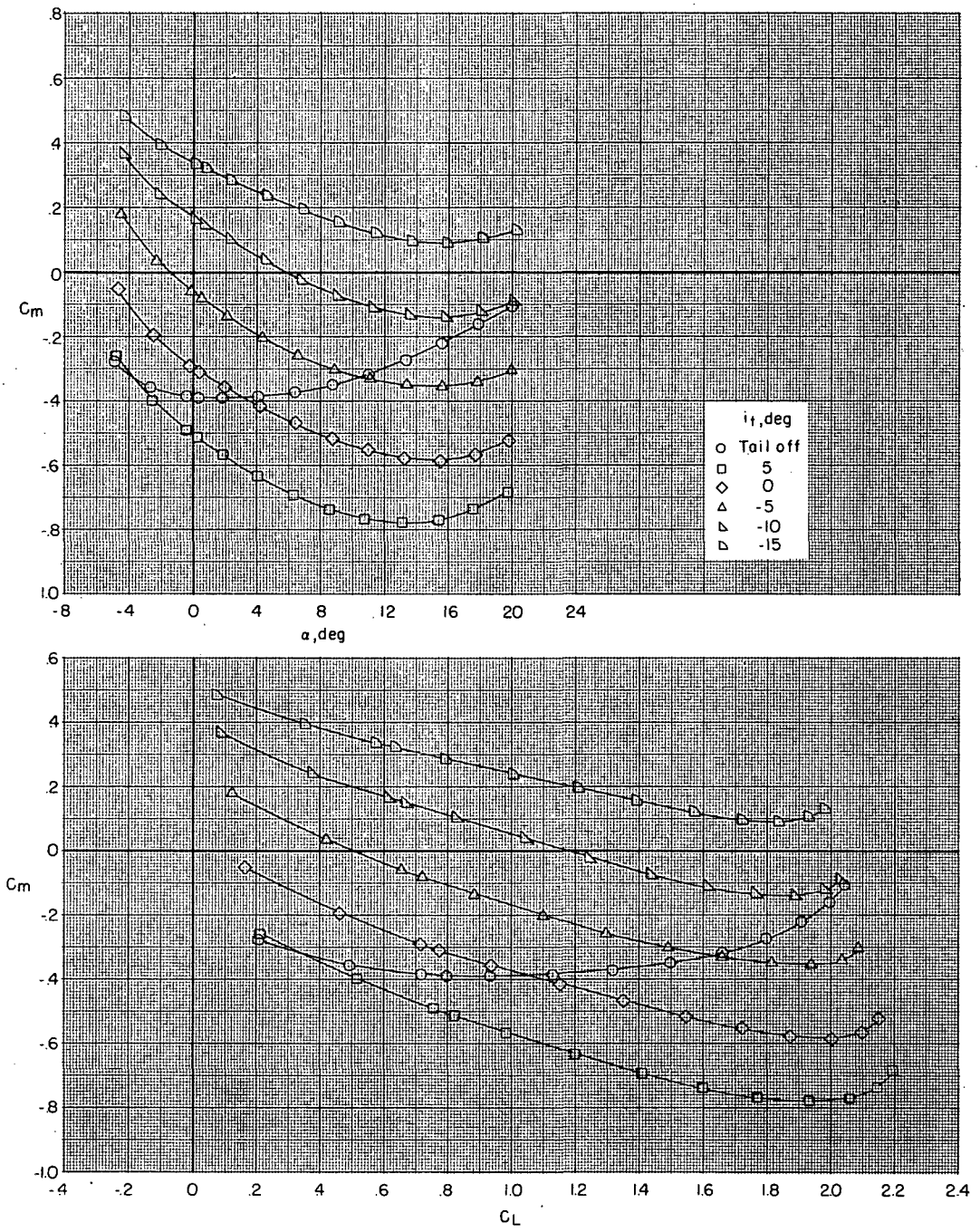

Figure 6.- Concluded.

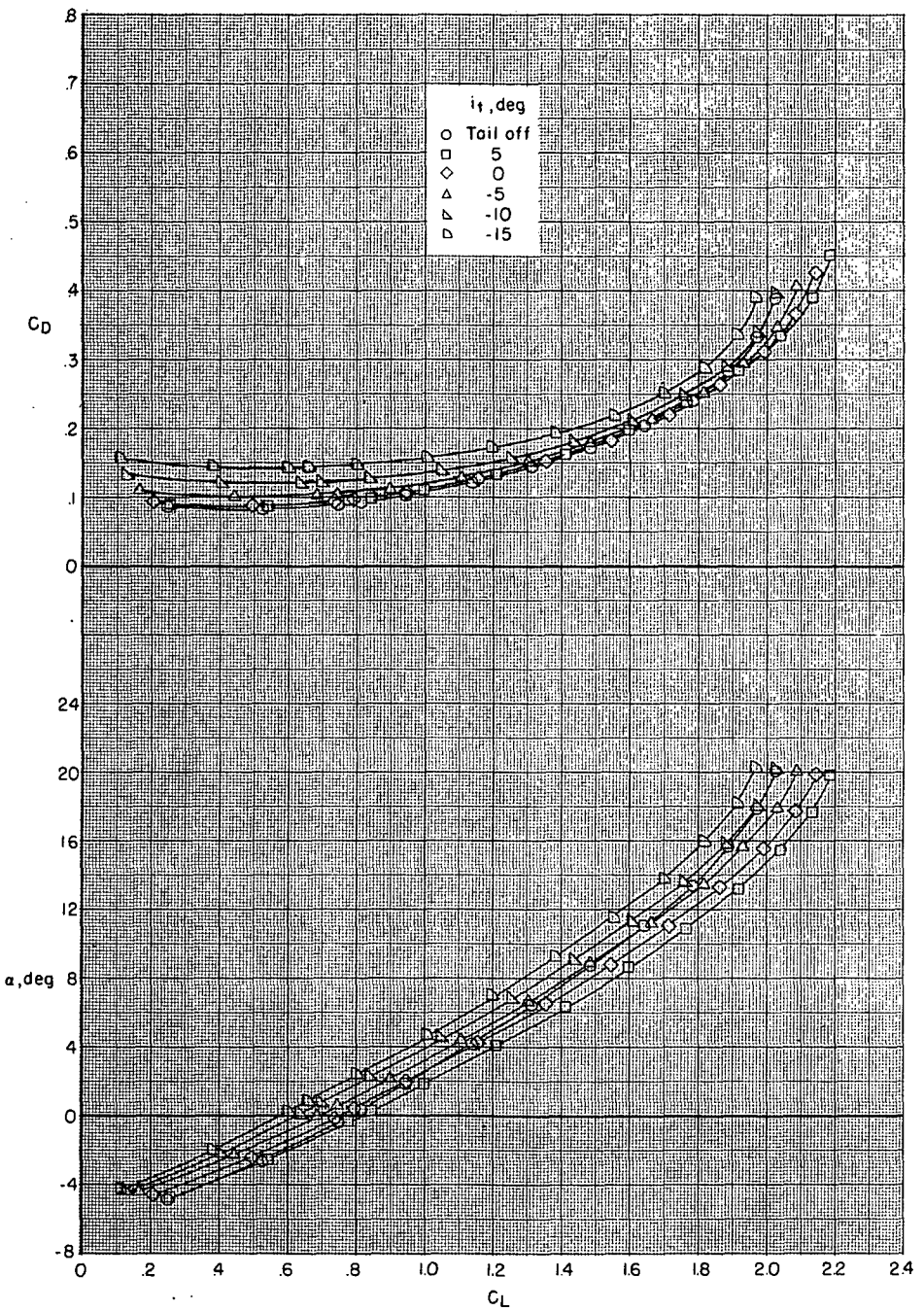

Figure 7.- Effect of horizontal-tail deflection on longitudinal aerodynamic characteristics of take-off configuration with nacelles off. $\delta_s = 40^o$; $\delta_f = 20^o$.

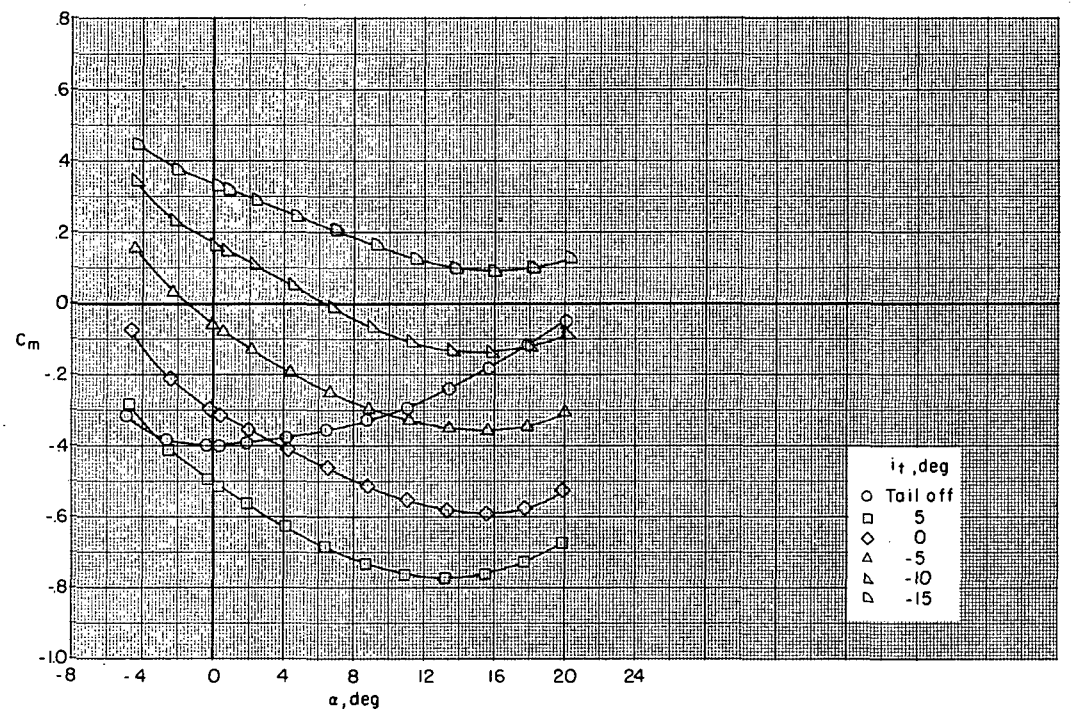

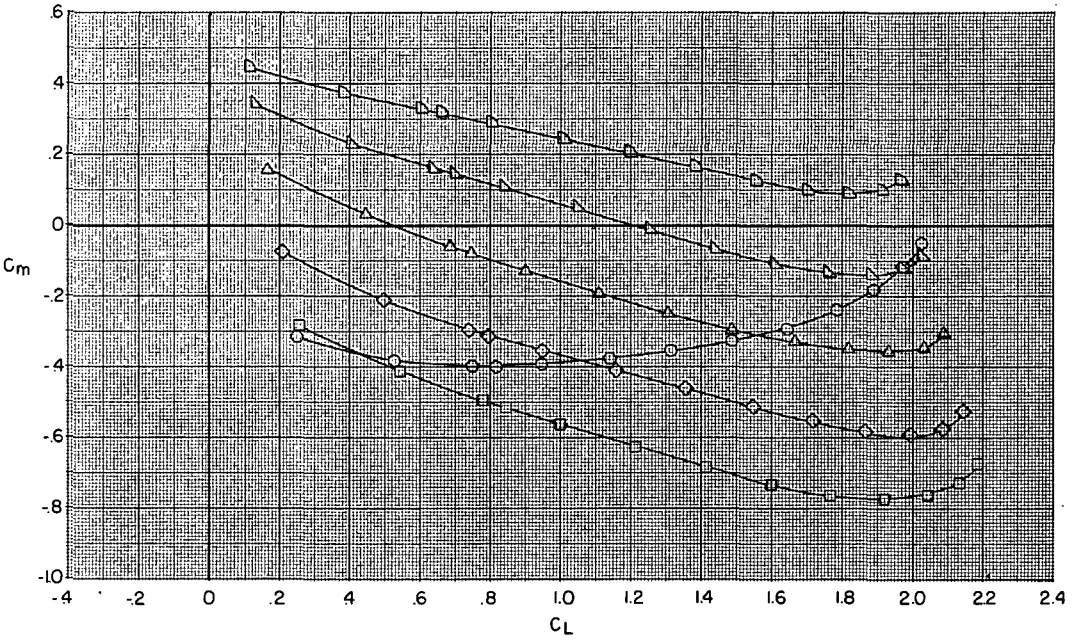

Figure 7.- Concluded.

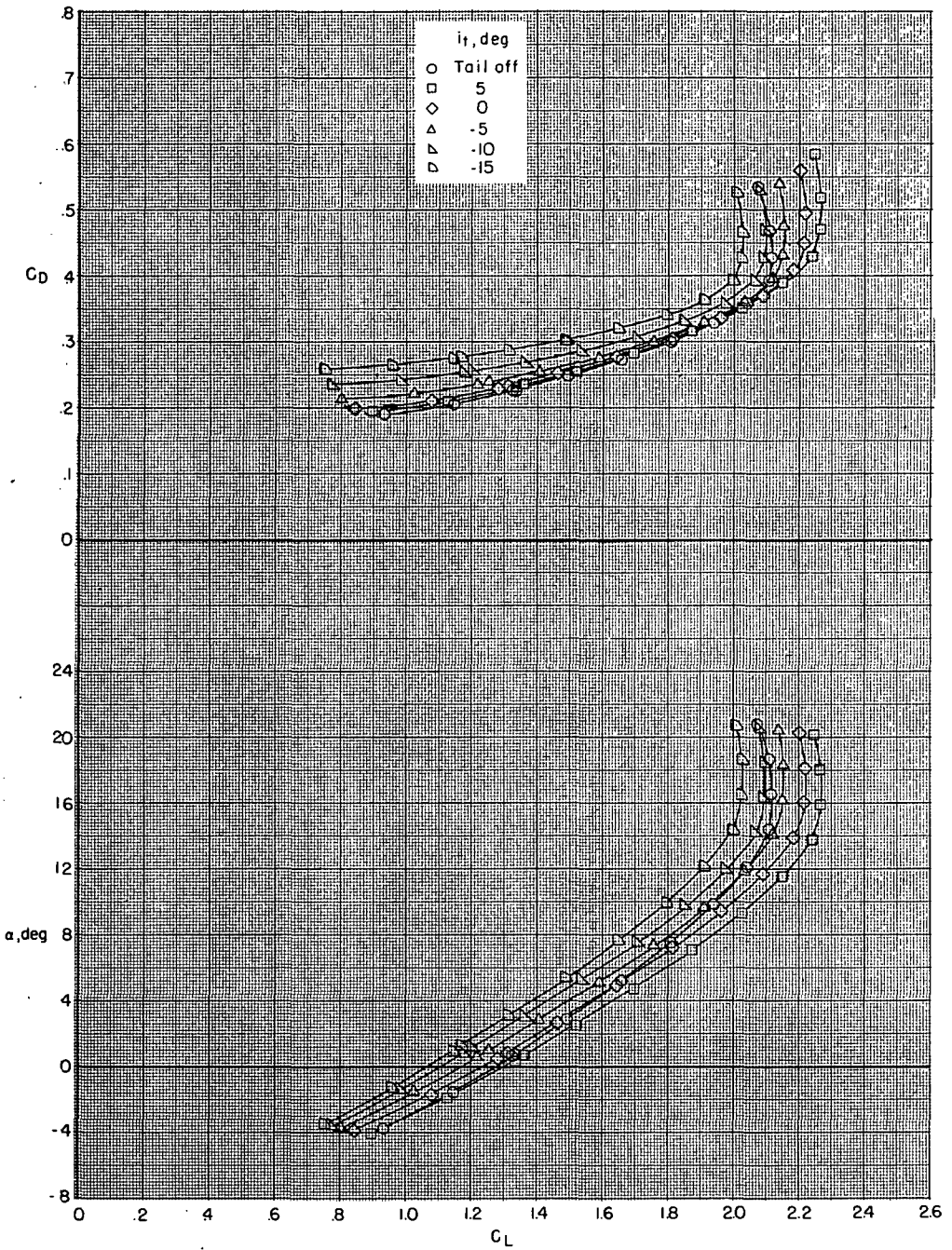

Figure 8.- Effect of horizontal-tail deflection on longitudinal aerodynamic characteristics of landing configuration with nacelles on. $\delta_s = 50^o$; $\delta_f = 40^o$.

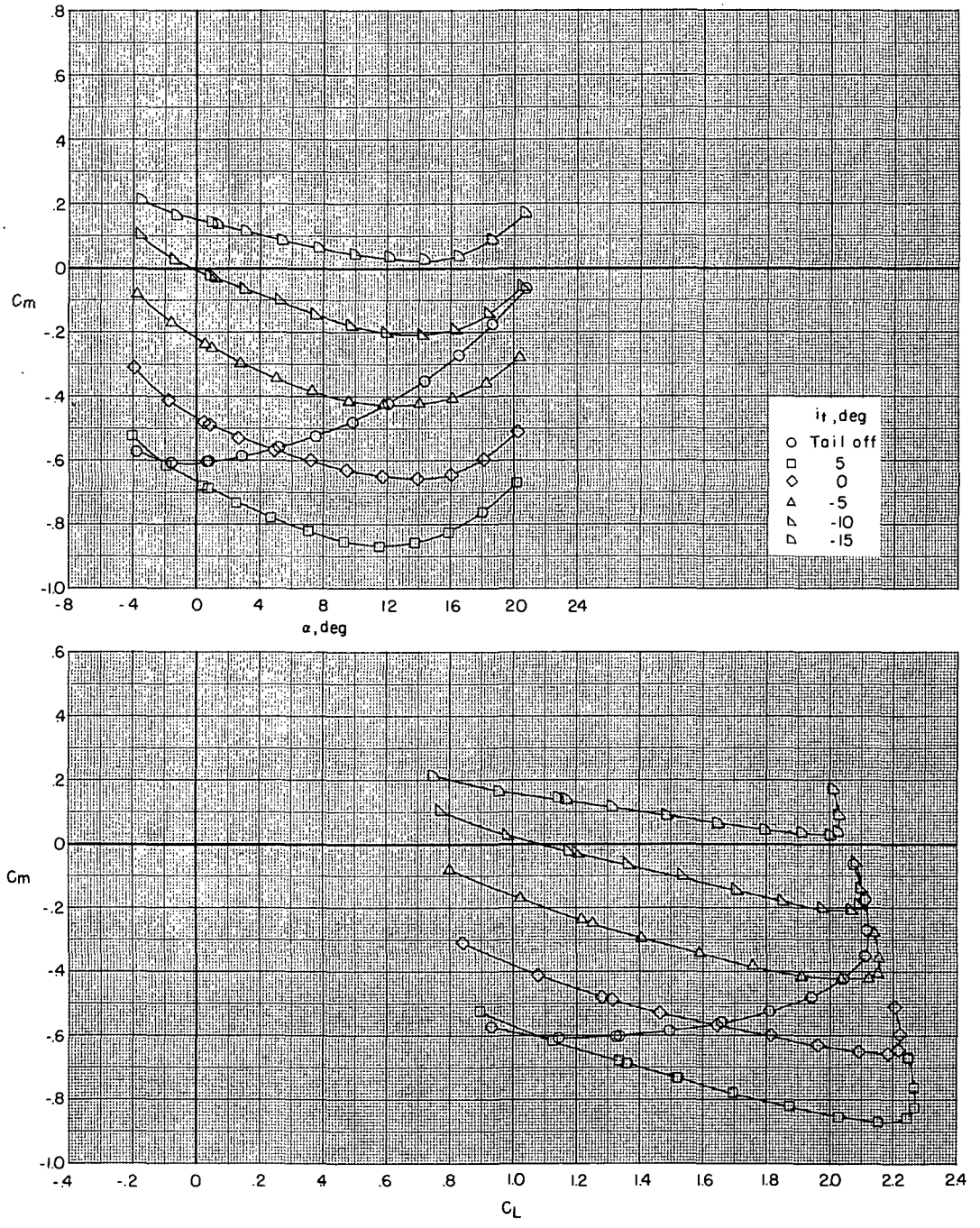

Figure 8.- Concluded.

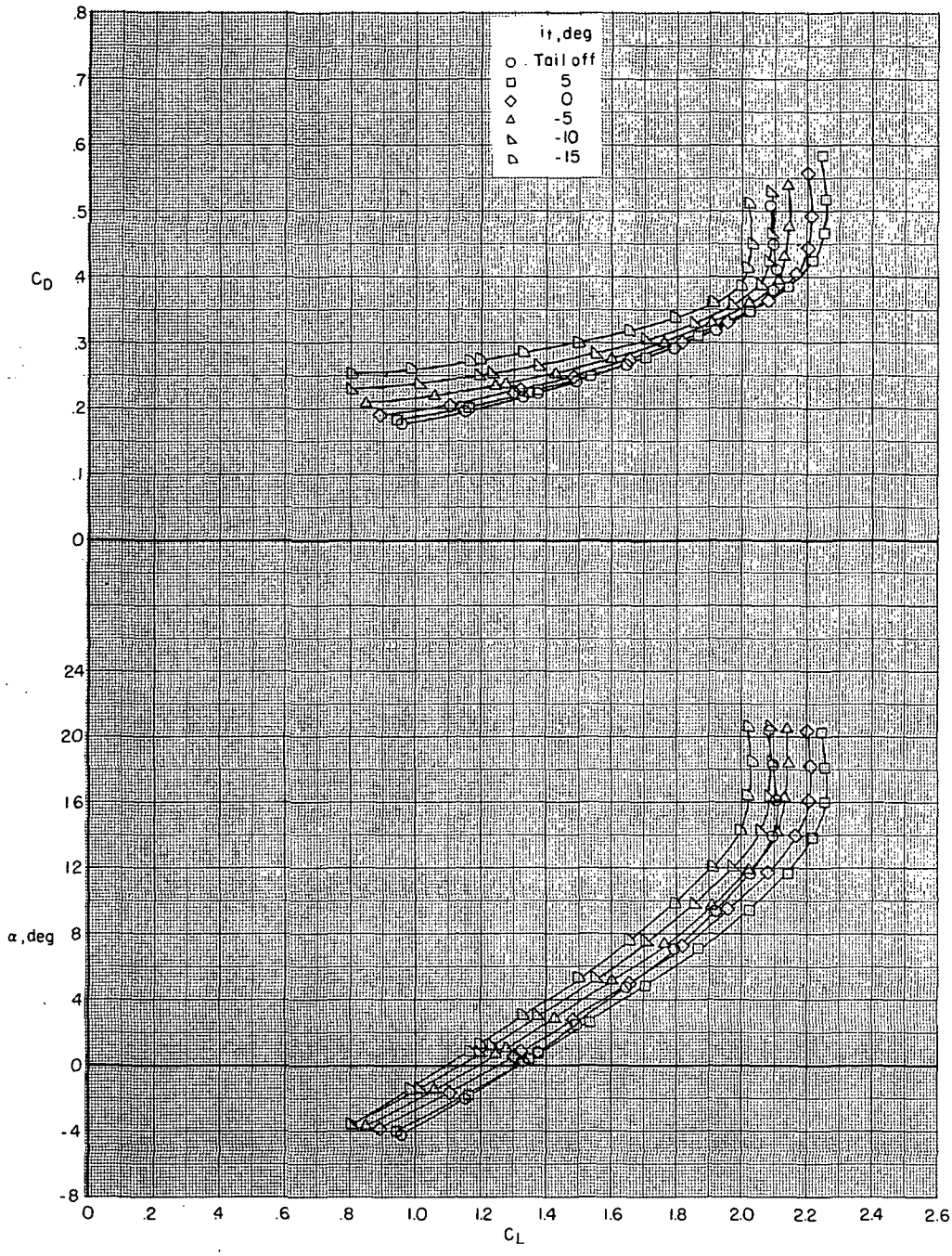

Figure 9.- Effect of horizontal-tail deflection on longitudinal aerodynamic characteristics of landing configuration with nacelles off. $\delta_s = 50^o$; $\delta_f = 40^o$.

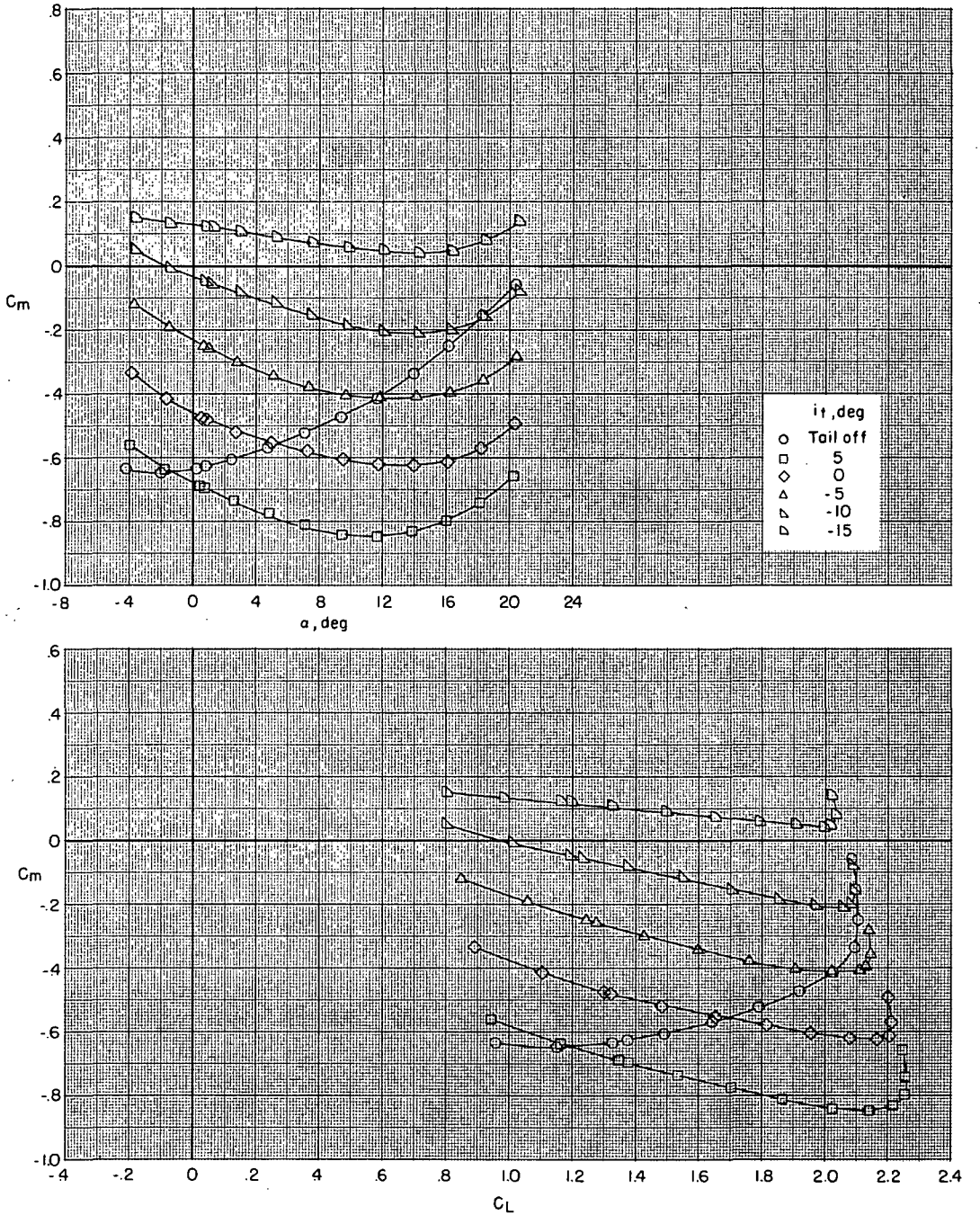

Figure 9.- Concluded.

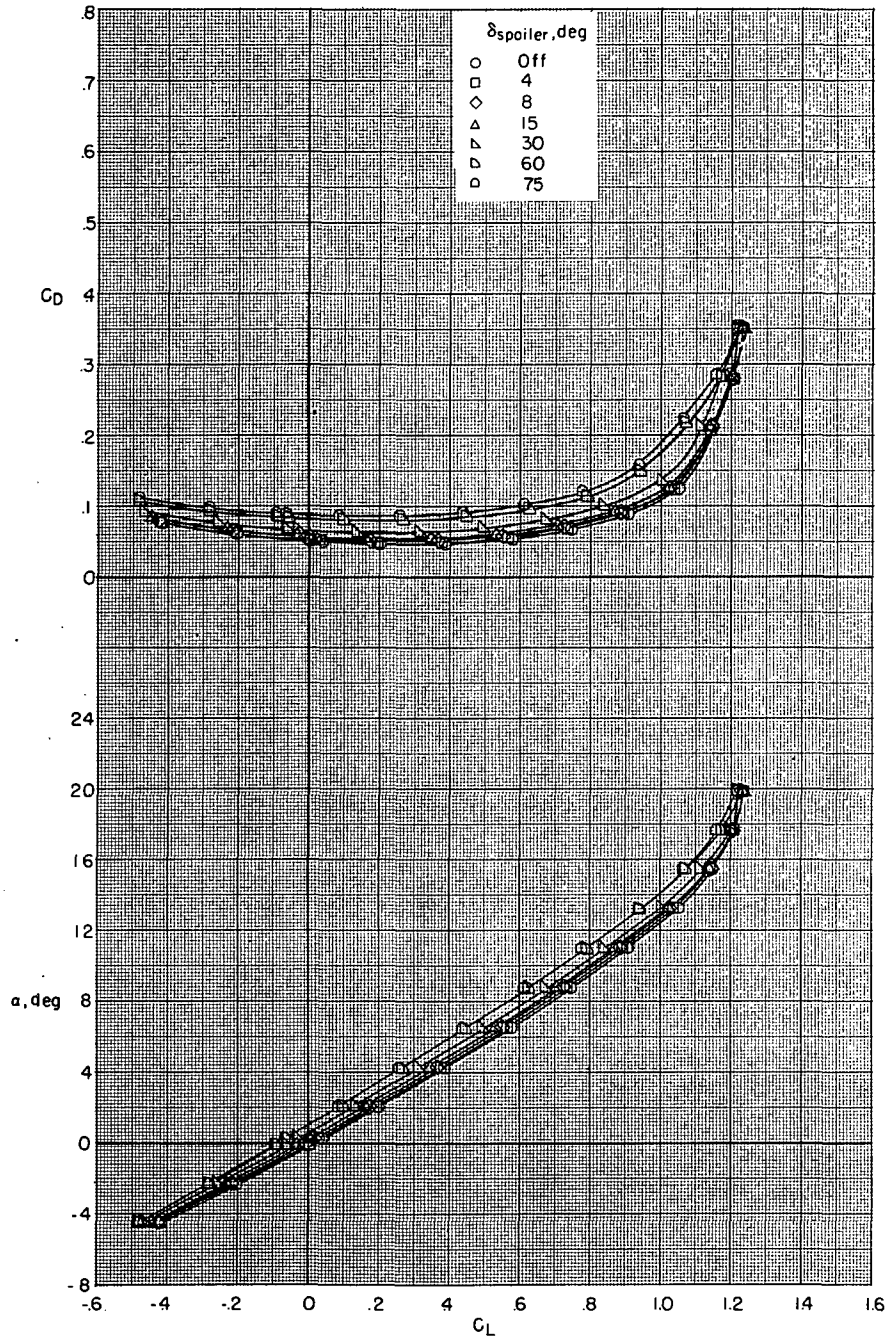

Figure 10.- Effect of wing upper-surface spoiler deflection for roll control for clean configuration with nacelles on and slat off. $i_t = -10^o$; $\delta_f = 0^o$.

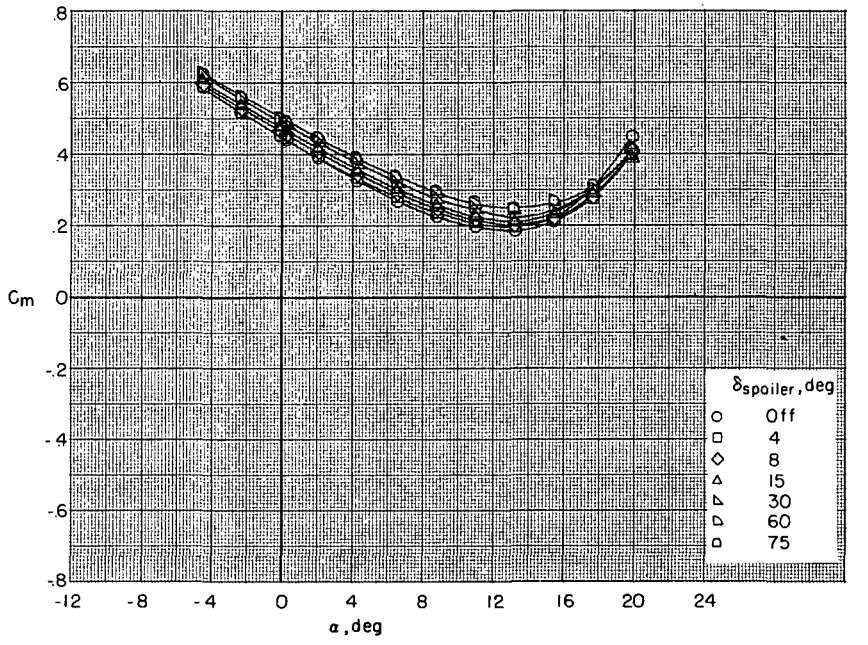

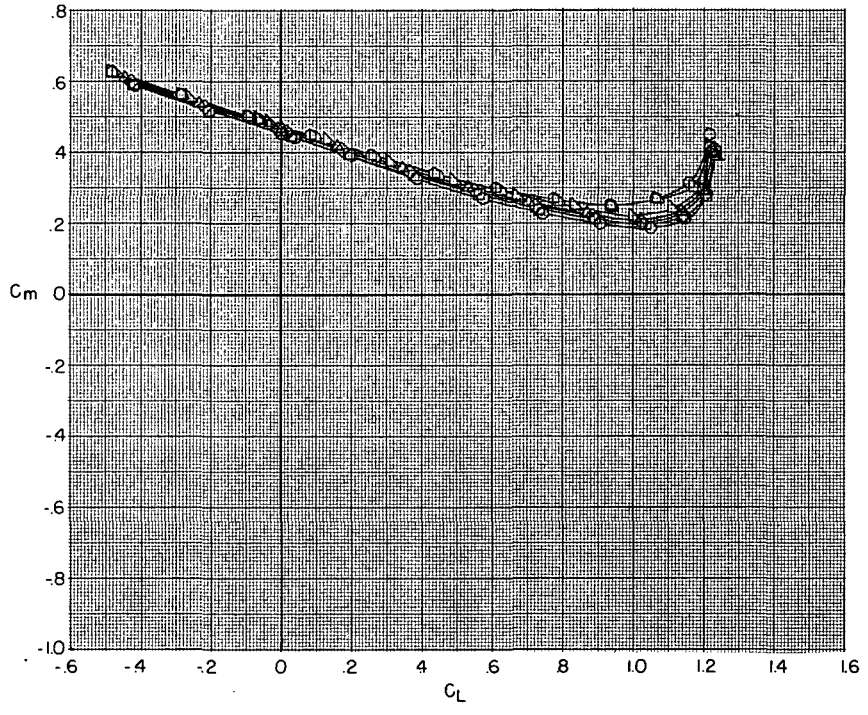

Figure 10.- Continued.

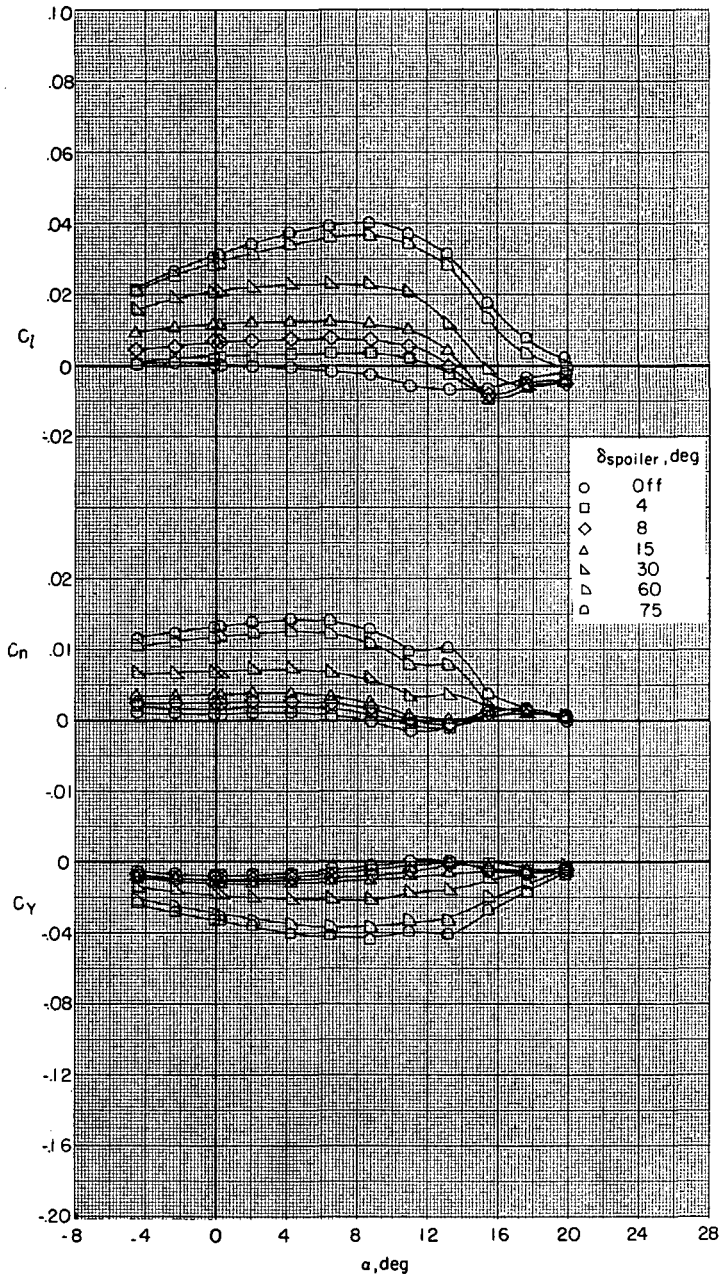

Figure 10.- Continued.

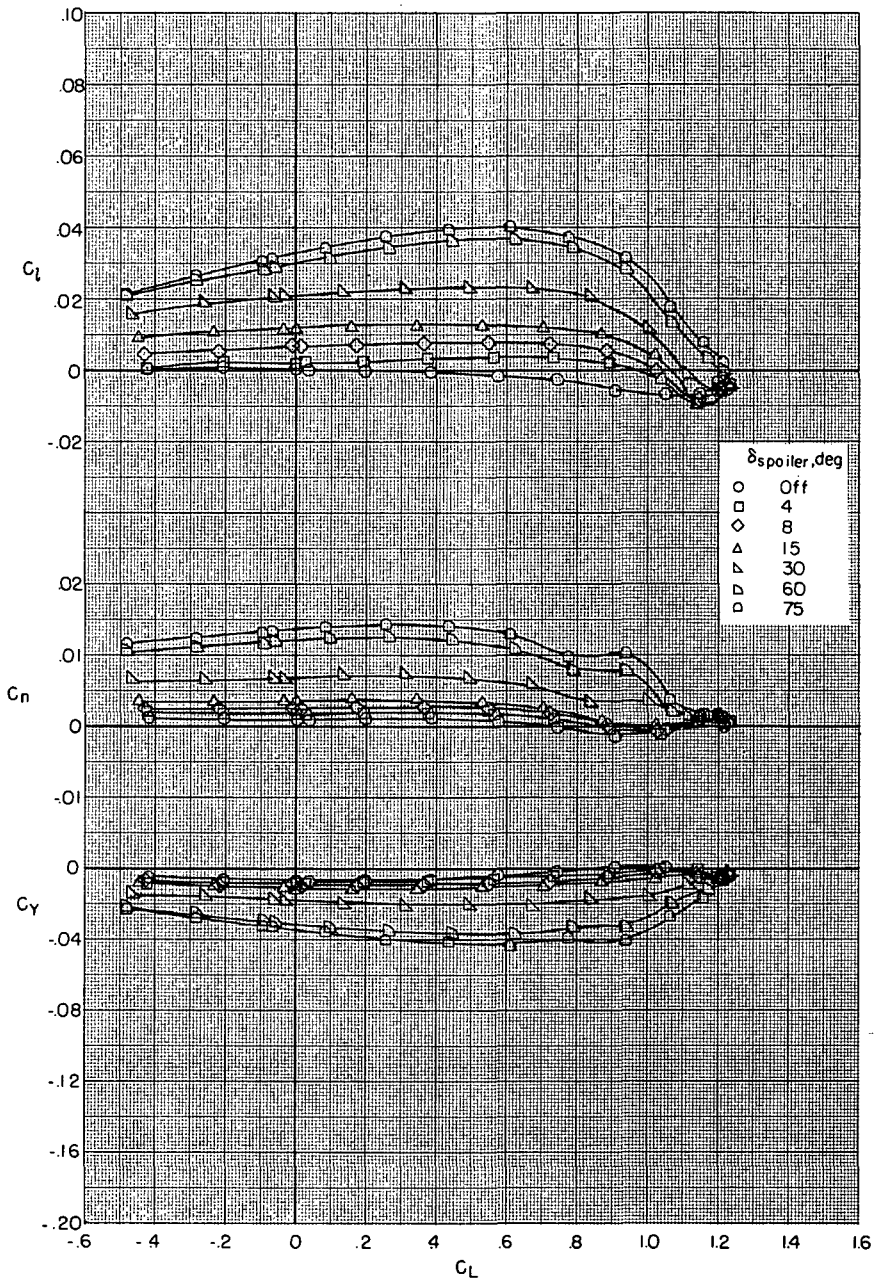

Figure 10.- Concluded.

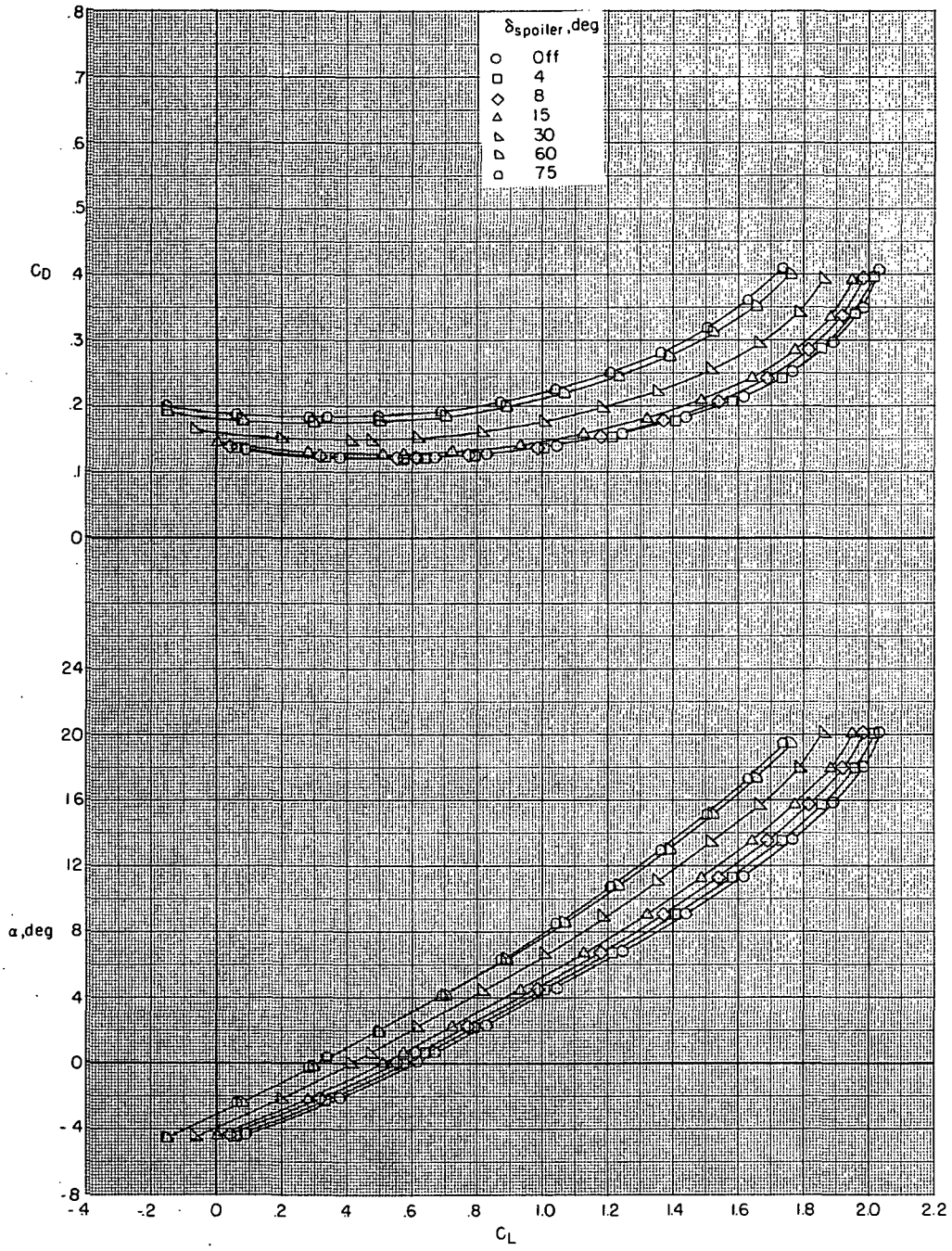

Figure 11.- Effect of wing upper-surface spoiler deflection for roll control for take-off configuration with nacelles on. $i_t = -10^o$; $\delta_s = 40^o$; $\delta_f = 20^o$.

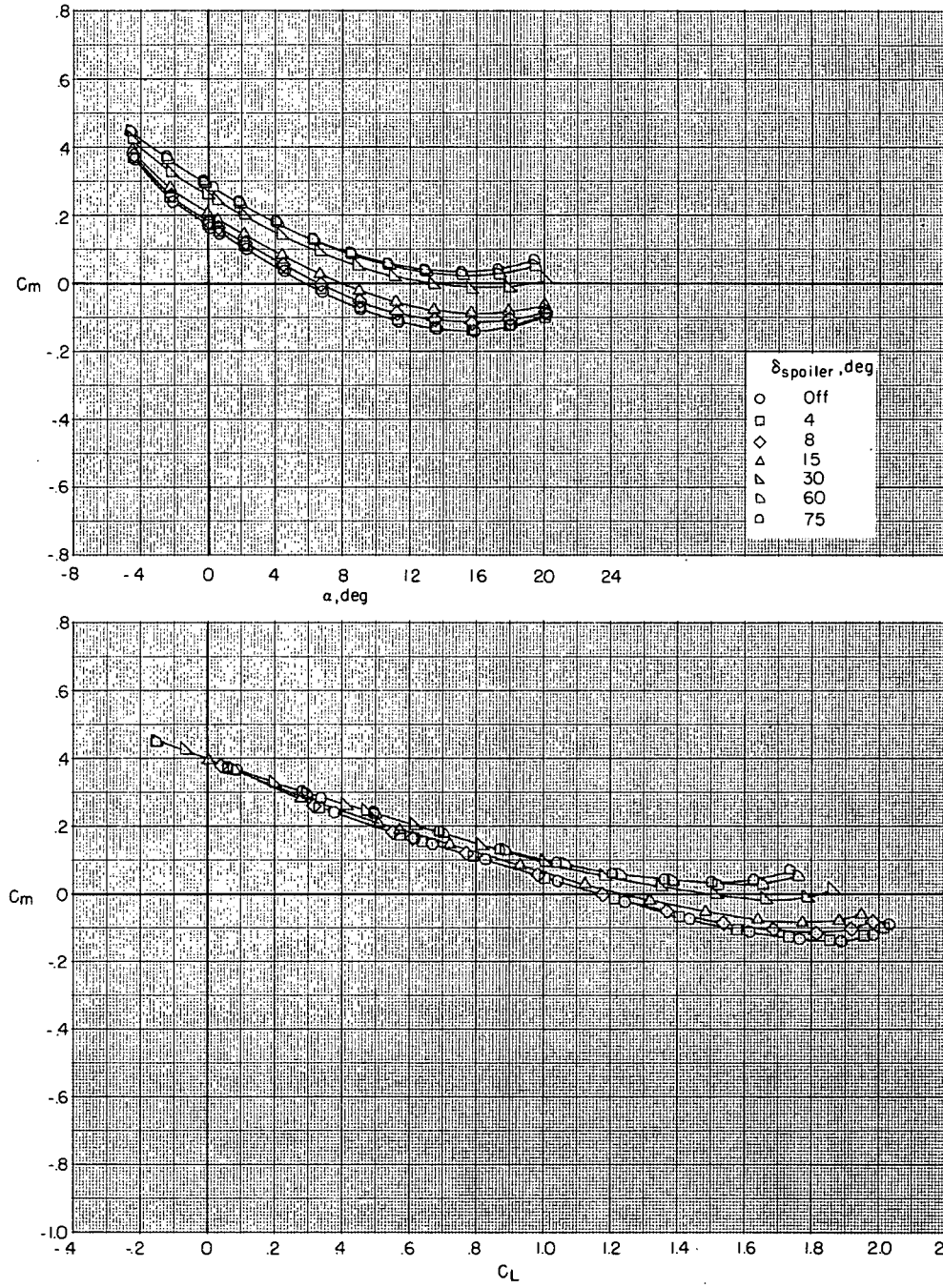

Figure 11.- Continued.

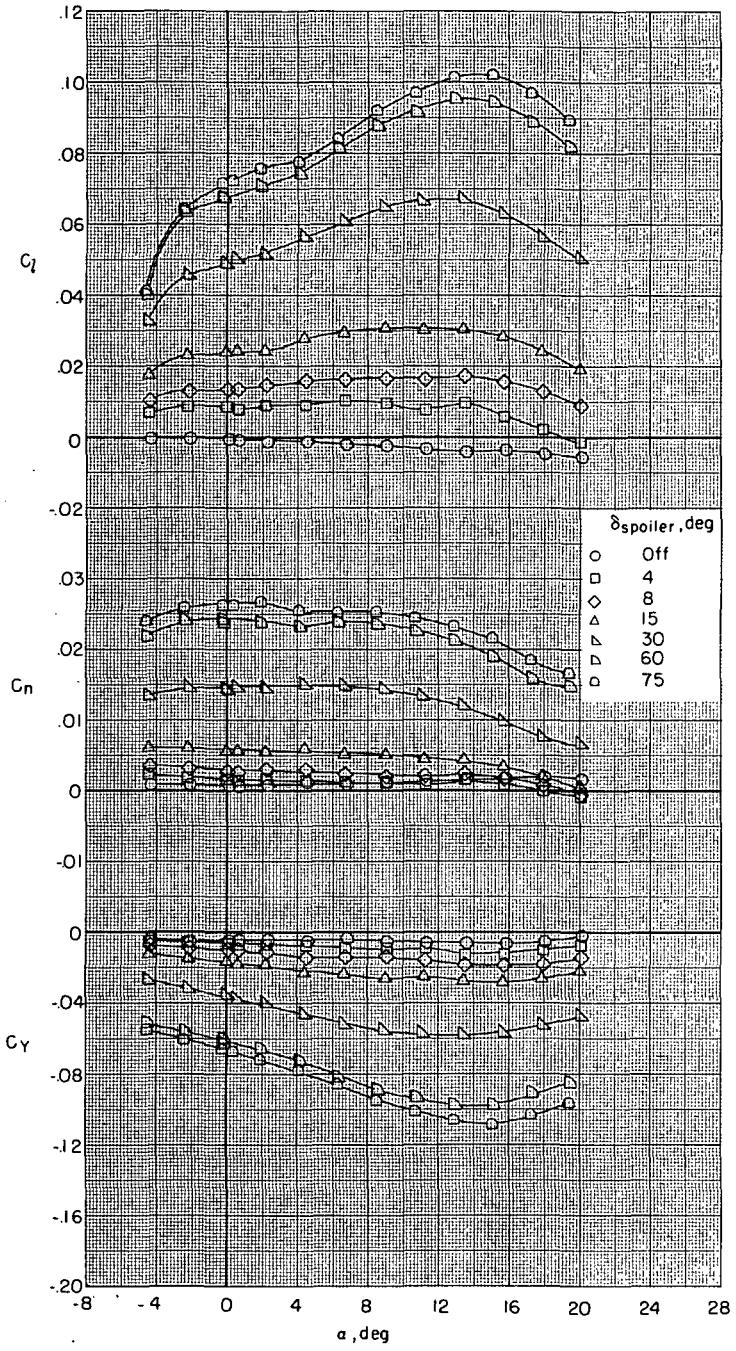

Figure 11.- Continued.

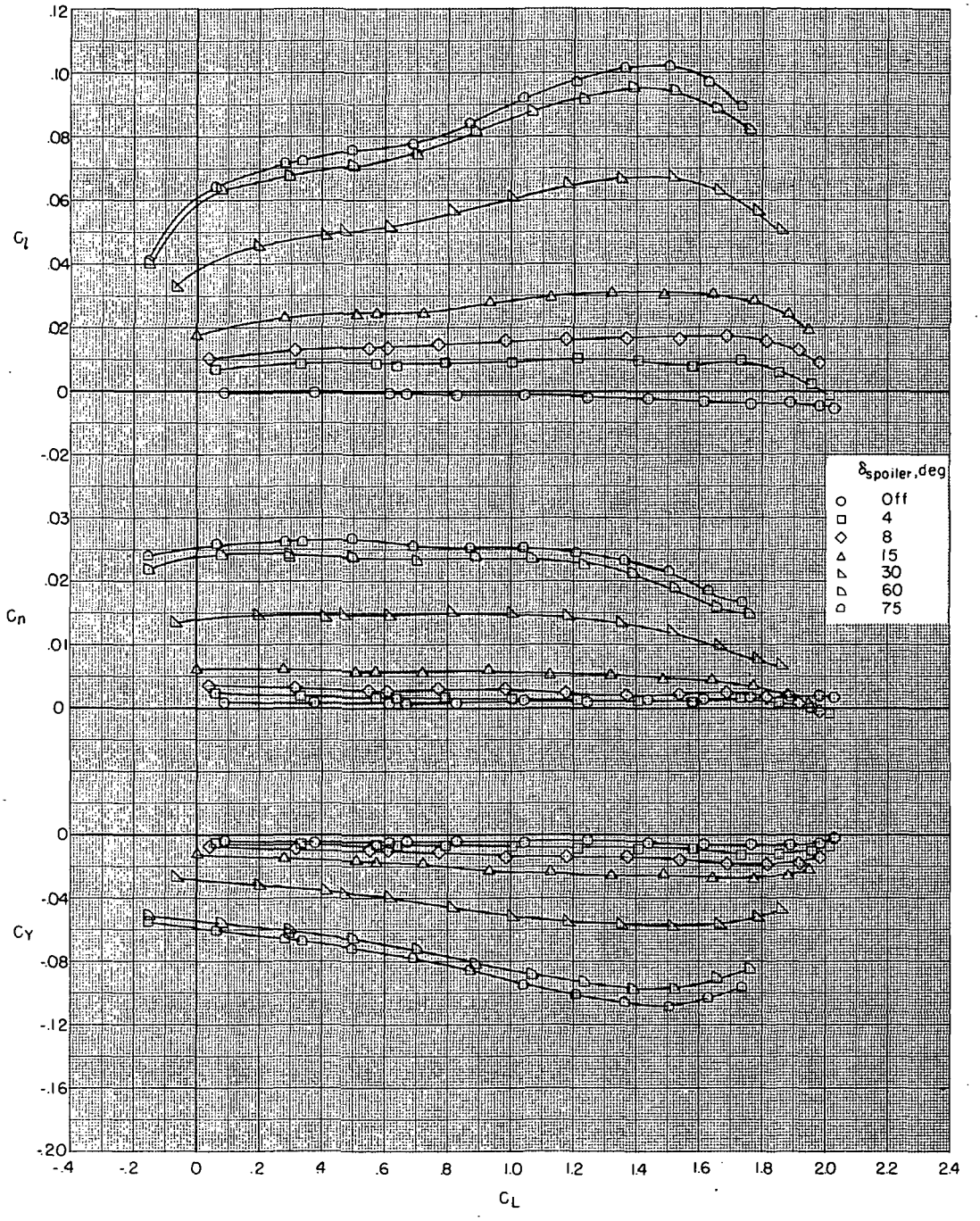

Figure 11.- Concluded.

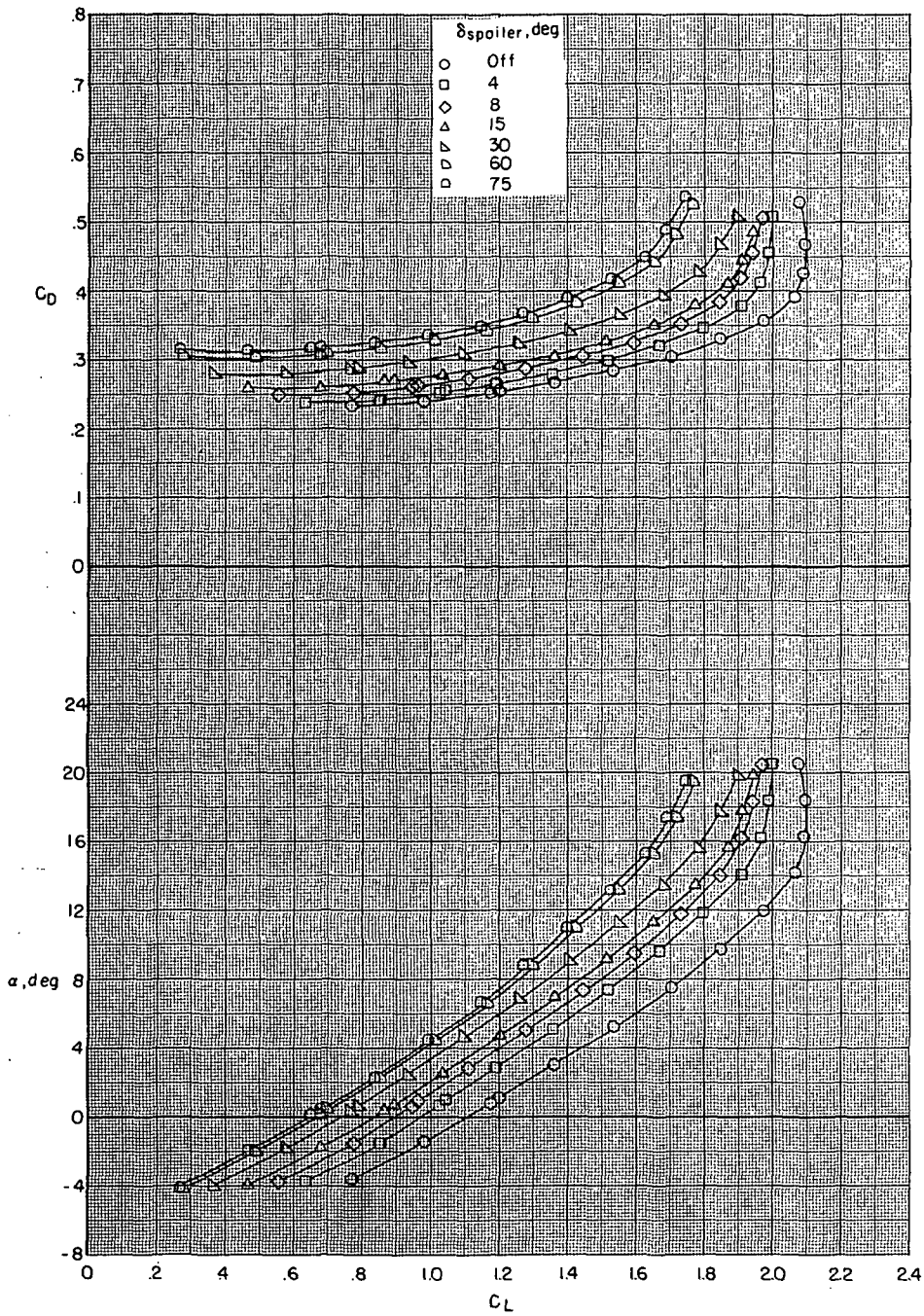

Figure 12.- Effect of wing upper-surface spoiler deflection for roll control for landing configuration with nacelles on. $i_t = -10^o$; $\delta_s = 50^o$; $\delta_f = 40^o$.

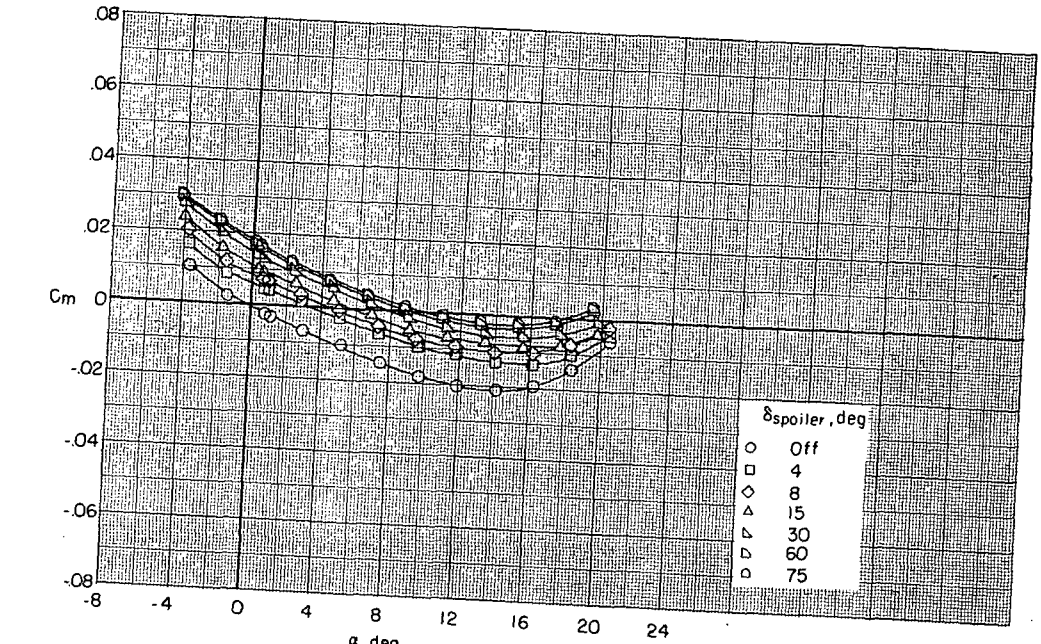

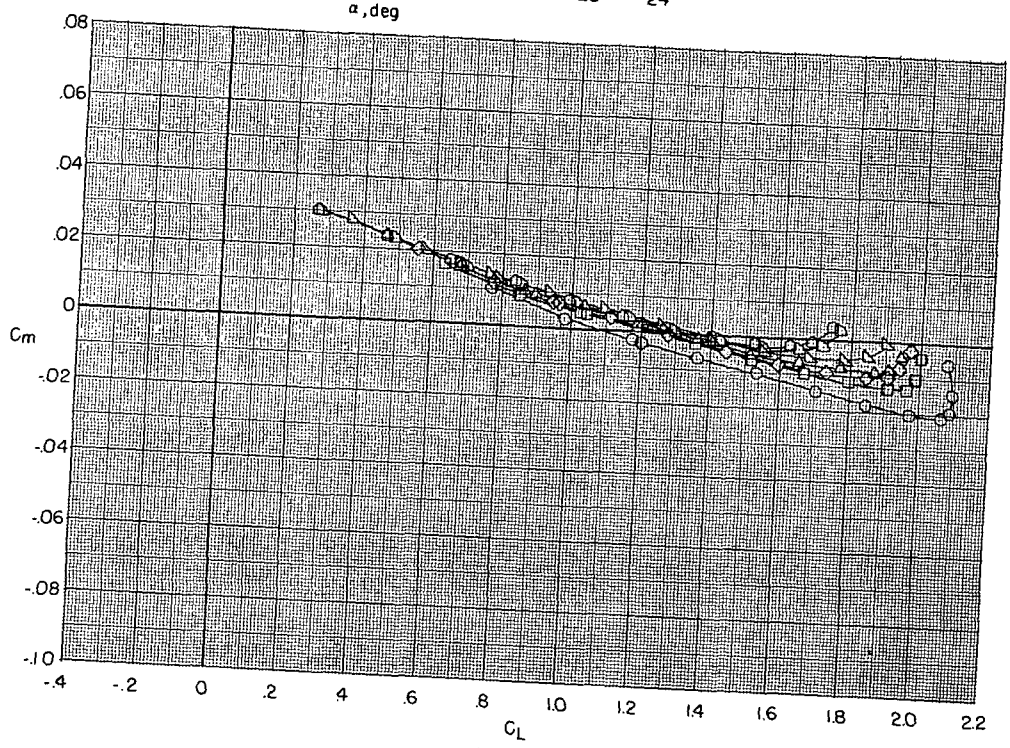

Figure 12.- Continued.

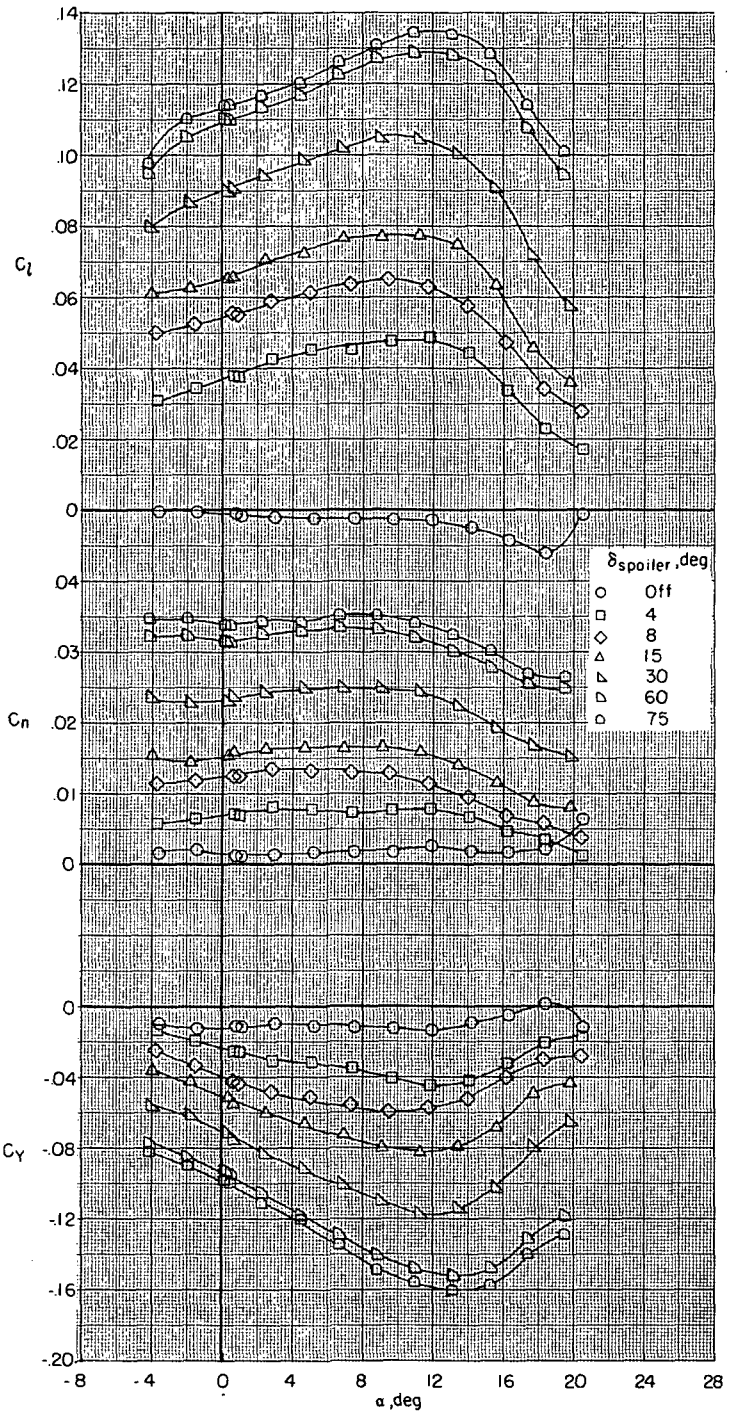

Figure 12.- Continued.

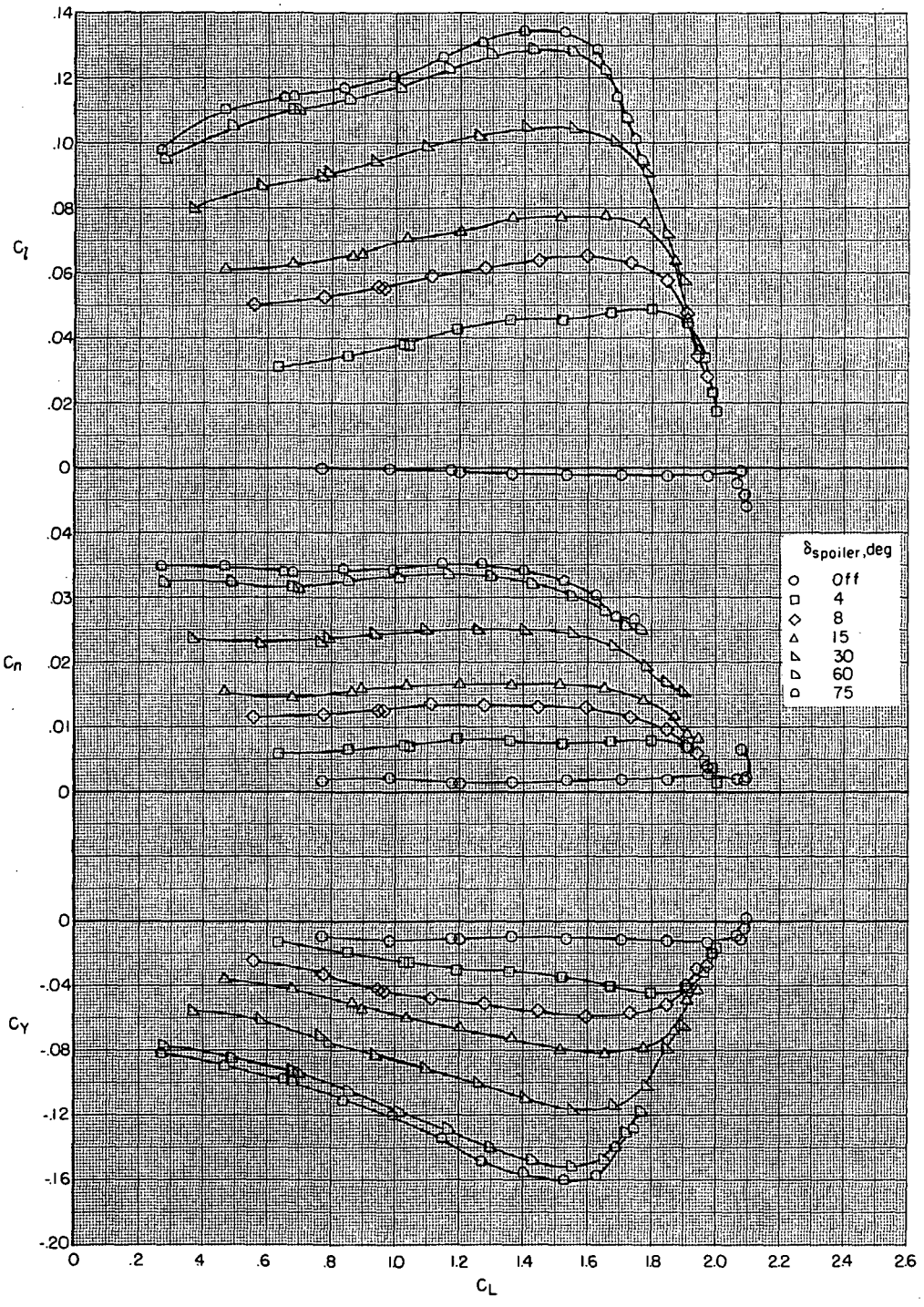

Figure 12.- Concluded.

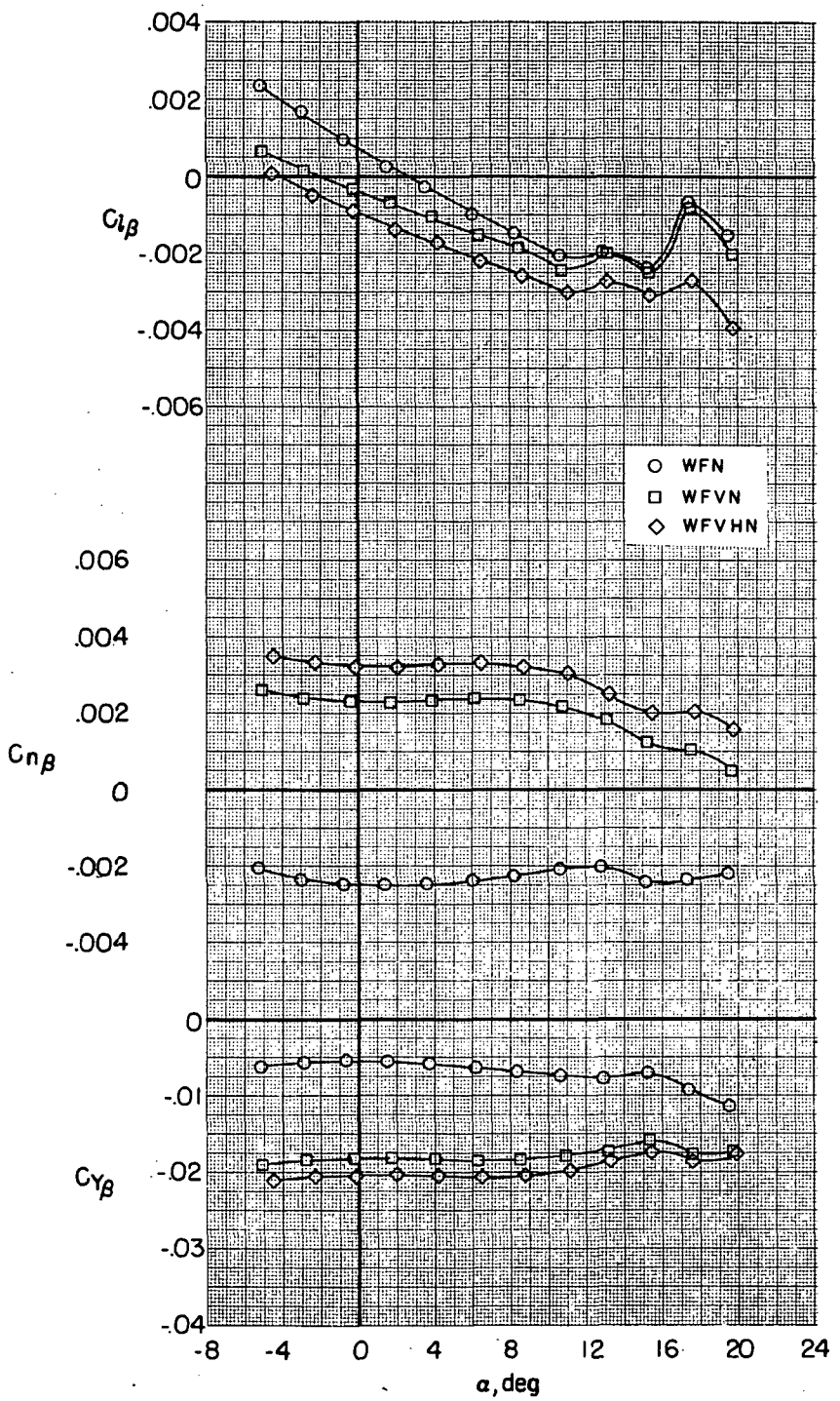

Figure 13.- Effect of horizontal and vertical tails on static lateral stability derivatives of clean configuration with nacelles on and slat off. $i_t = -10^o$ for horizontal tail on; $\delta_f = 0^o$.

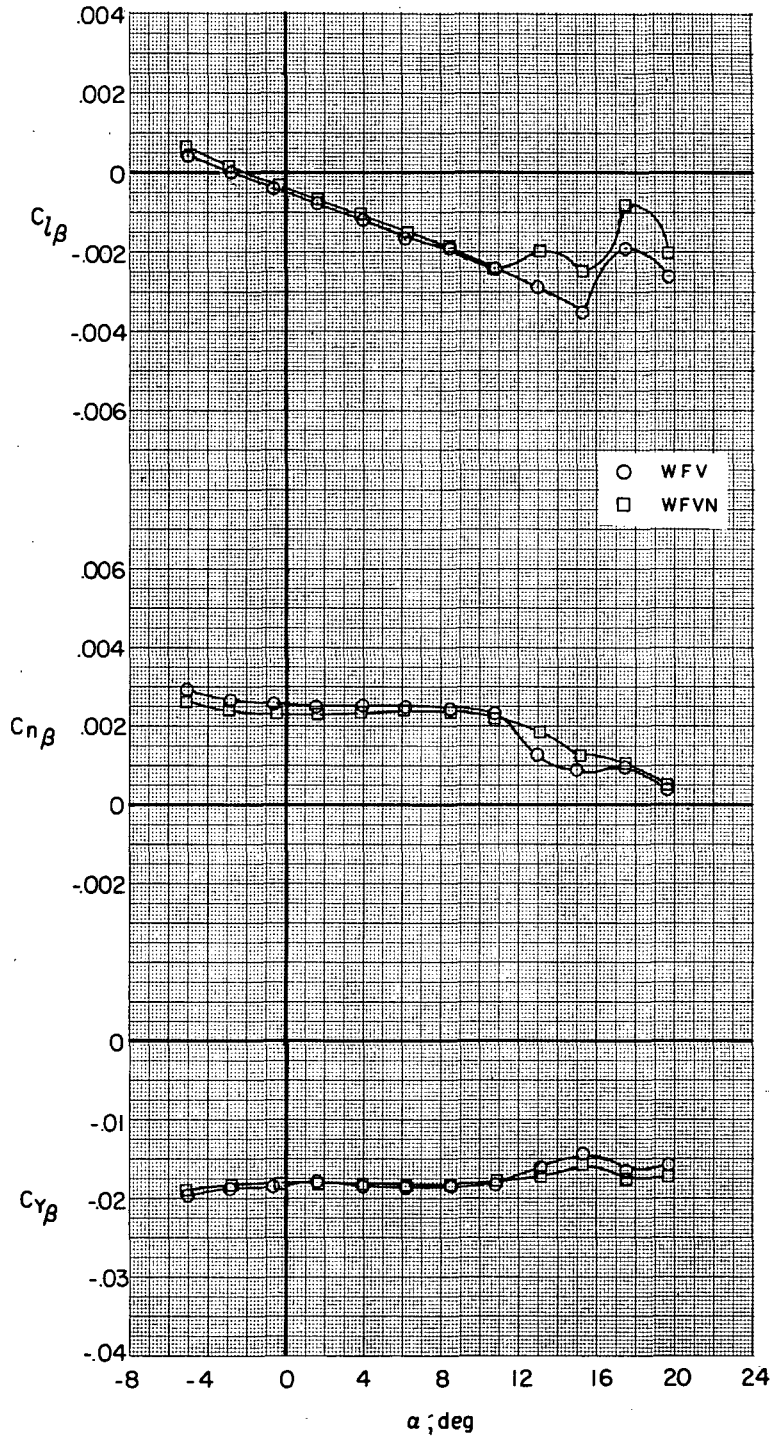

Figure 14.- Effect of nacelles on static lateral stability derivatives of clean configuration with slat and horizontal-tail surface removed. $\delta_f = 0^o$.

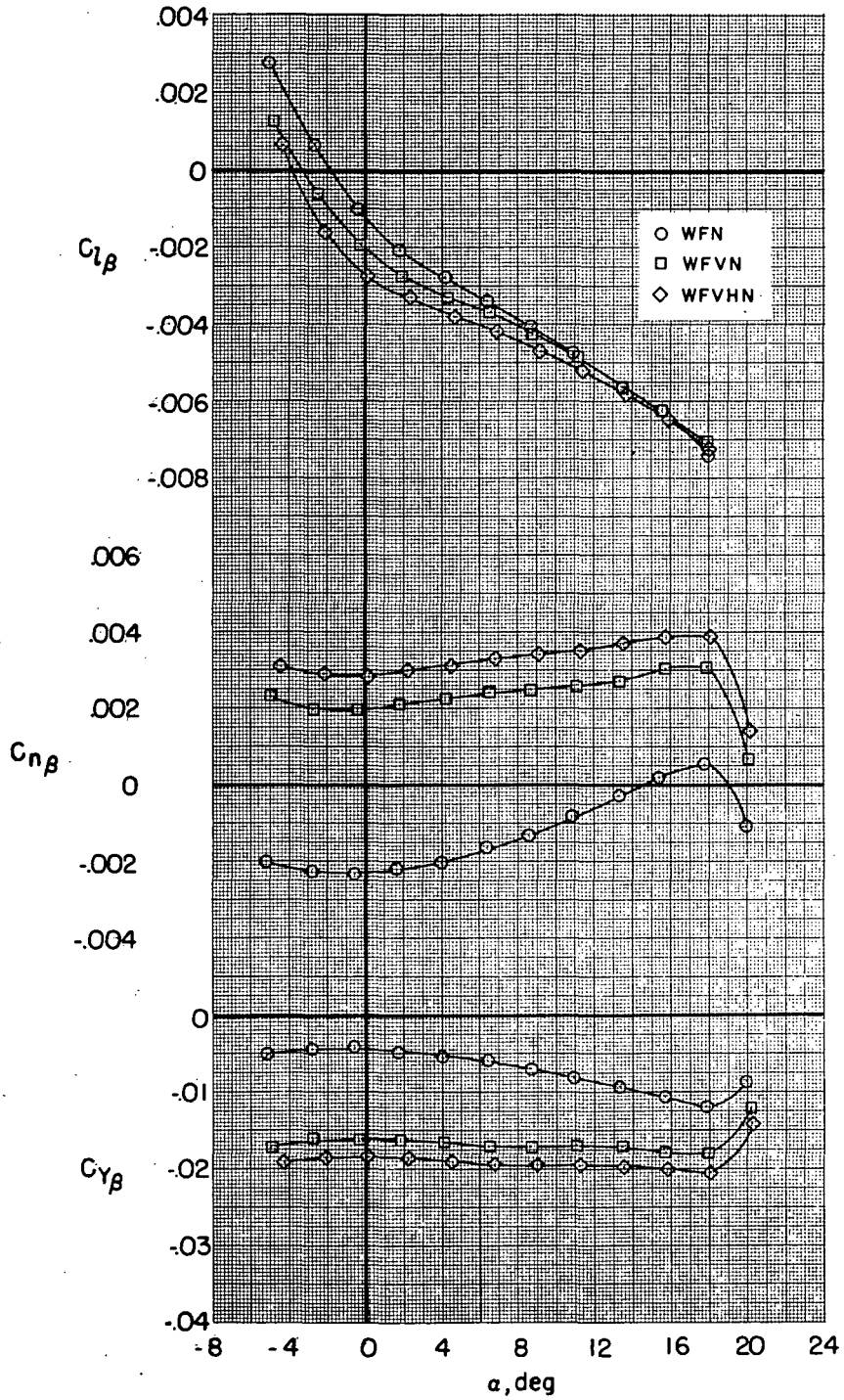

Figure 15.- Effect of horizontal and vertical tails on static lateral stability derivatives of take-off configuration with nacelles on. $i_t = -10^o$ for horizontal tail on; $\delta_s = 40^o$; $\delta_f = 20^o$.

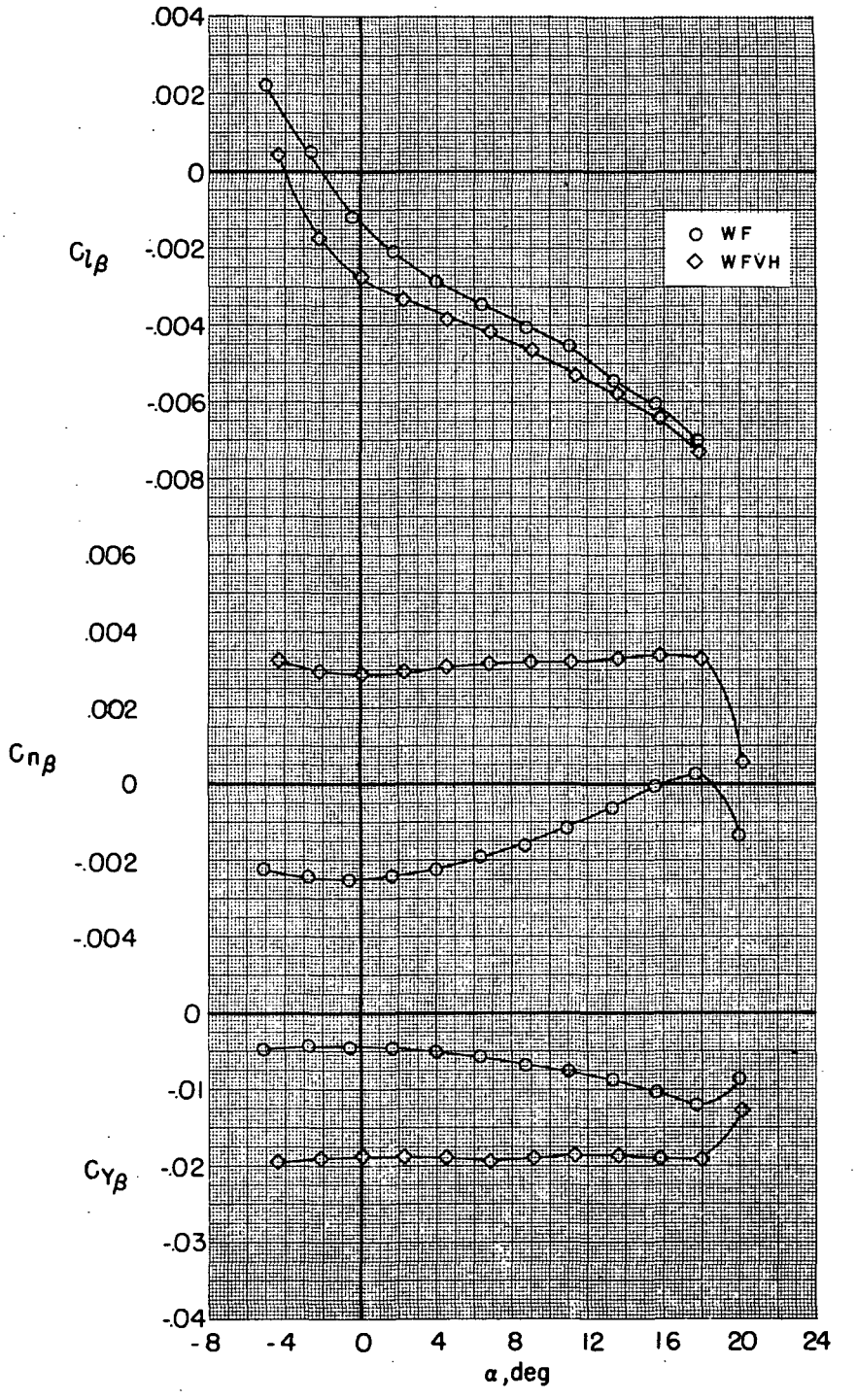

Figure 16.- Effect of horizontal and vertical tails on static lateral stability derivatives of take-off configuration with nacelles off. $i_t = -10^o$ for horizontal tail on; $\delta_s = 40^o$; $\delta_f = 20^o$.

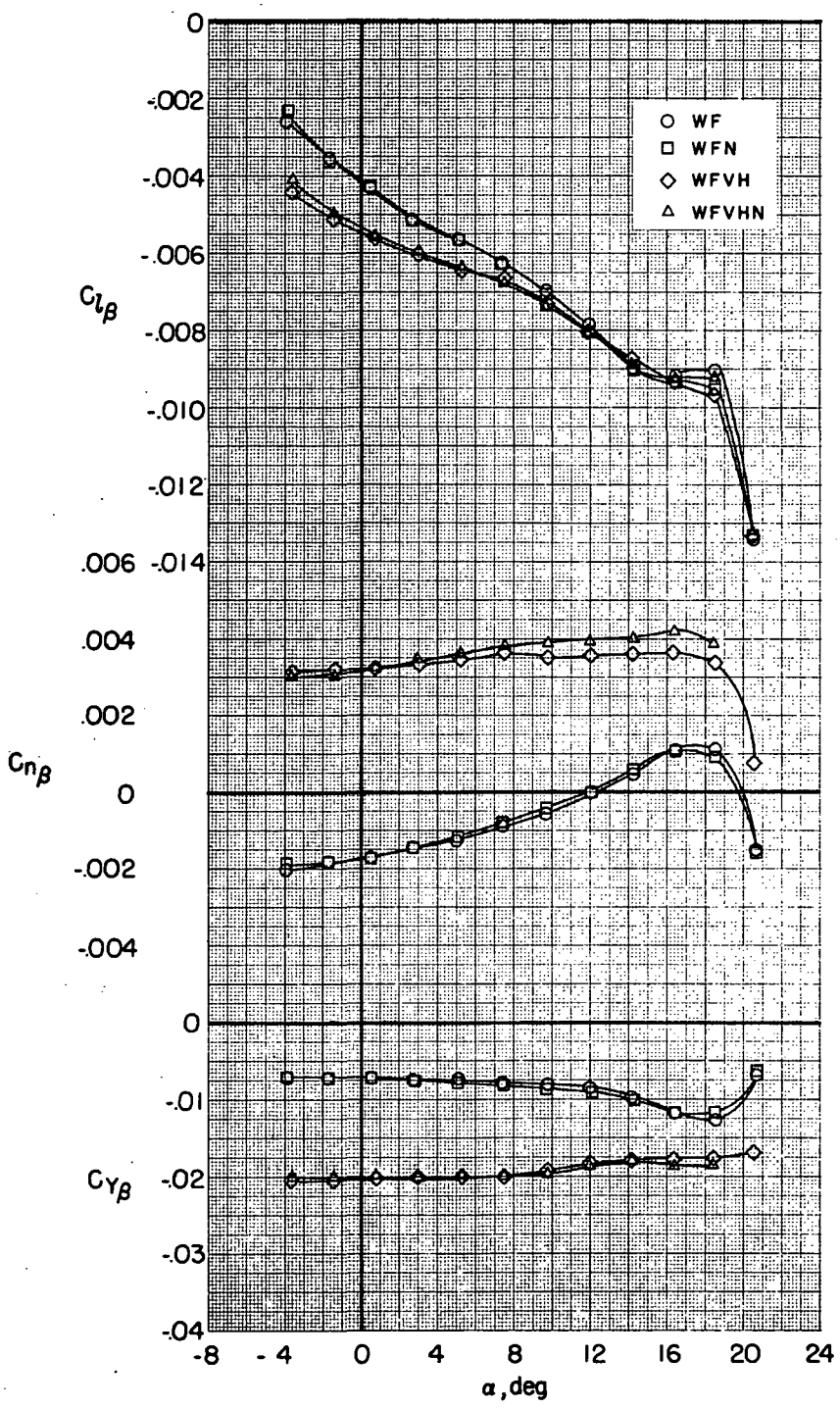

Figure 17.- Effect of horizontal and vertical tails on static lateral stability derivatives of landing configuration with and without nacelles. $i_t = -10^o$ for horizontal tail on; $\delta_s = 50^o$; $\delta_f = 40^o$.

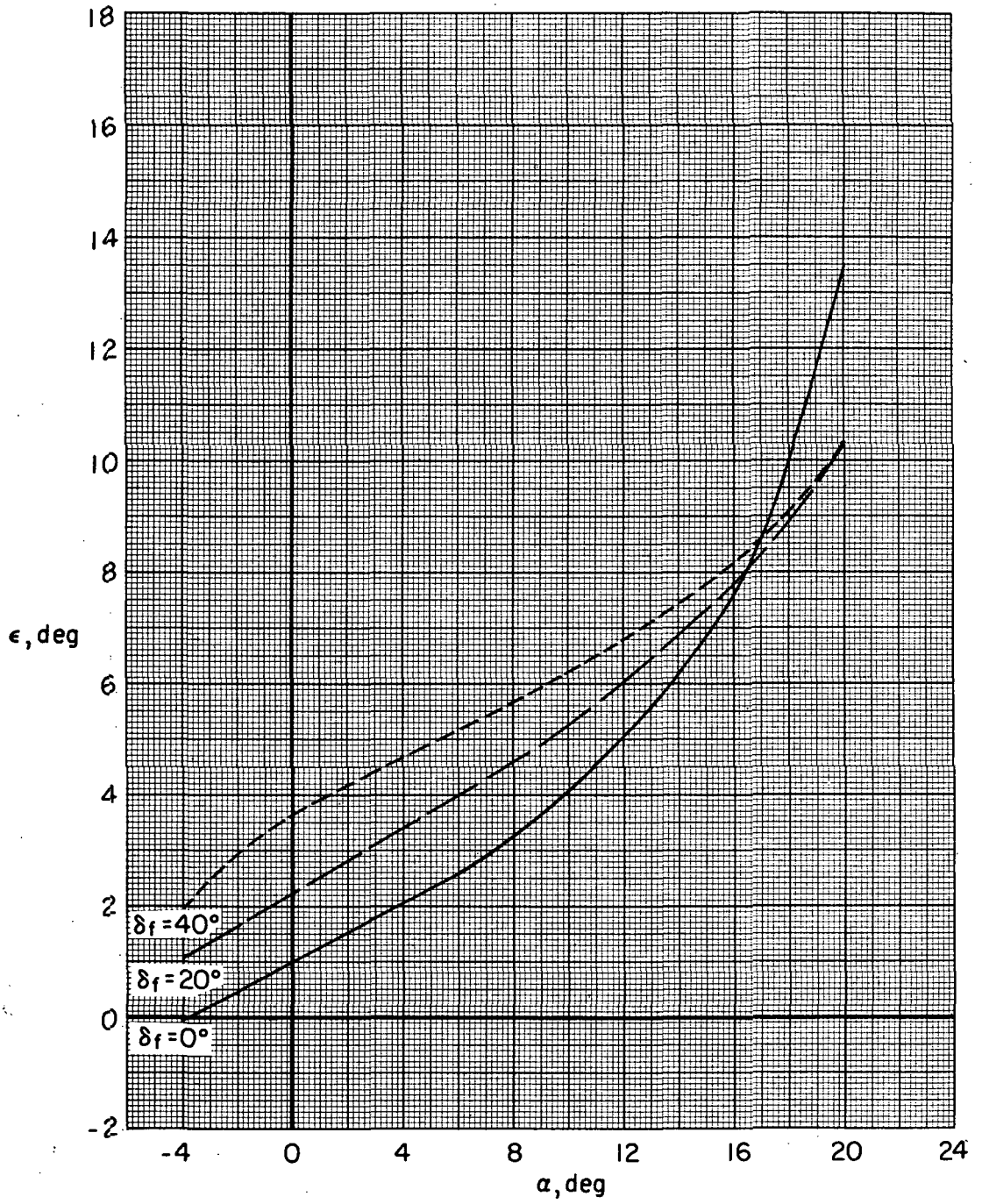

(a) Downwash angle.

Figure 18.- Effect of deflection of high-lift system on variation of effective downwash characteristics with angle of attack for model with nacelles on.

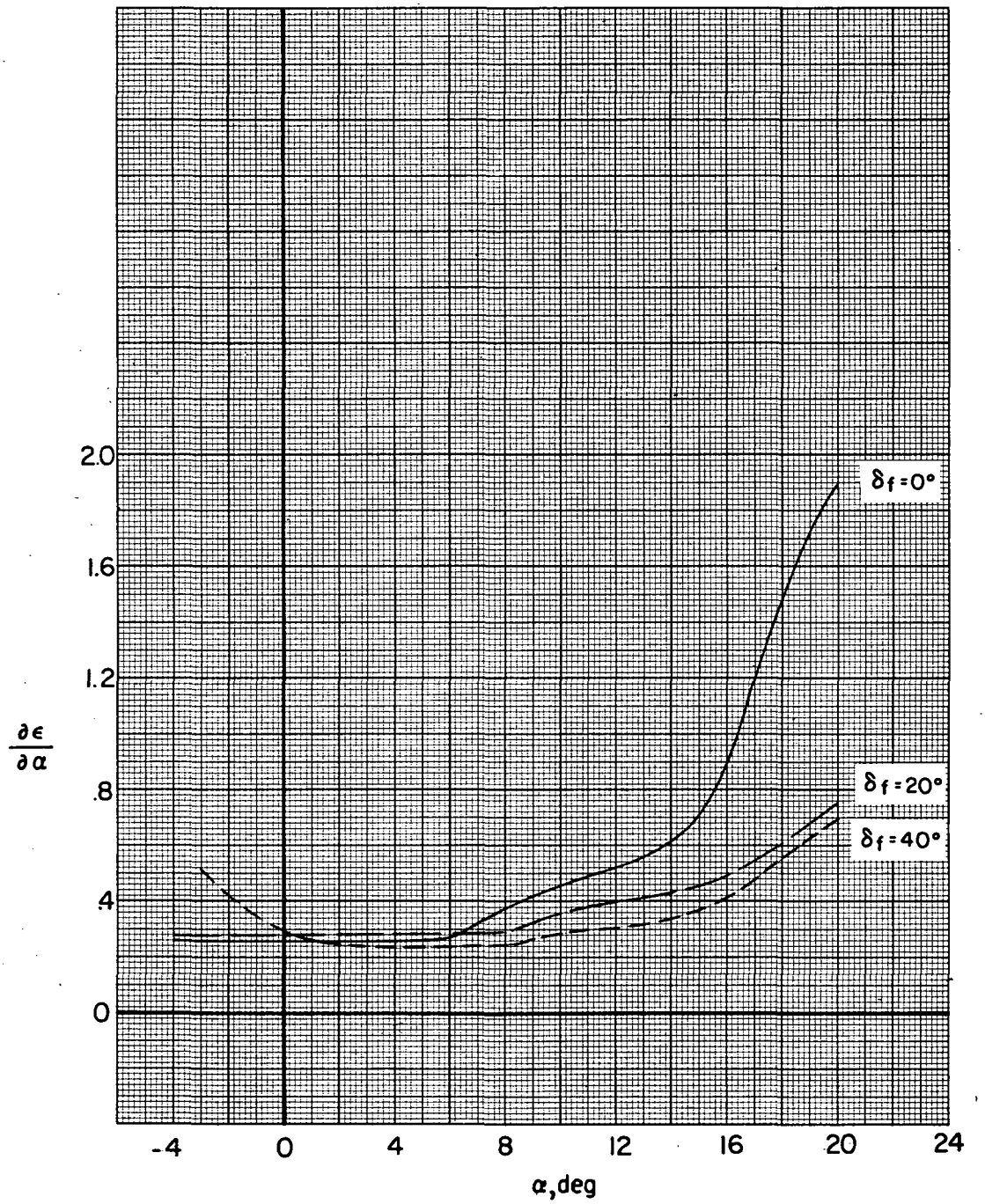

(b) Downwash slope, $\partial\epsilon/\partial\alpha$.

Figure 18.- Concluded.

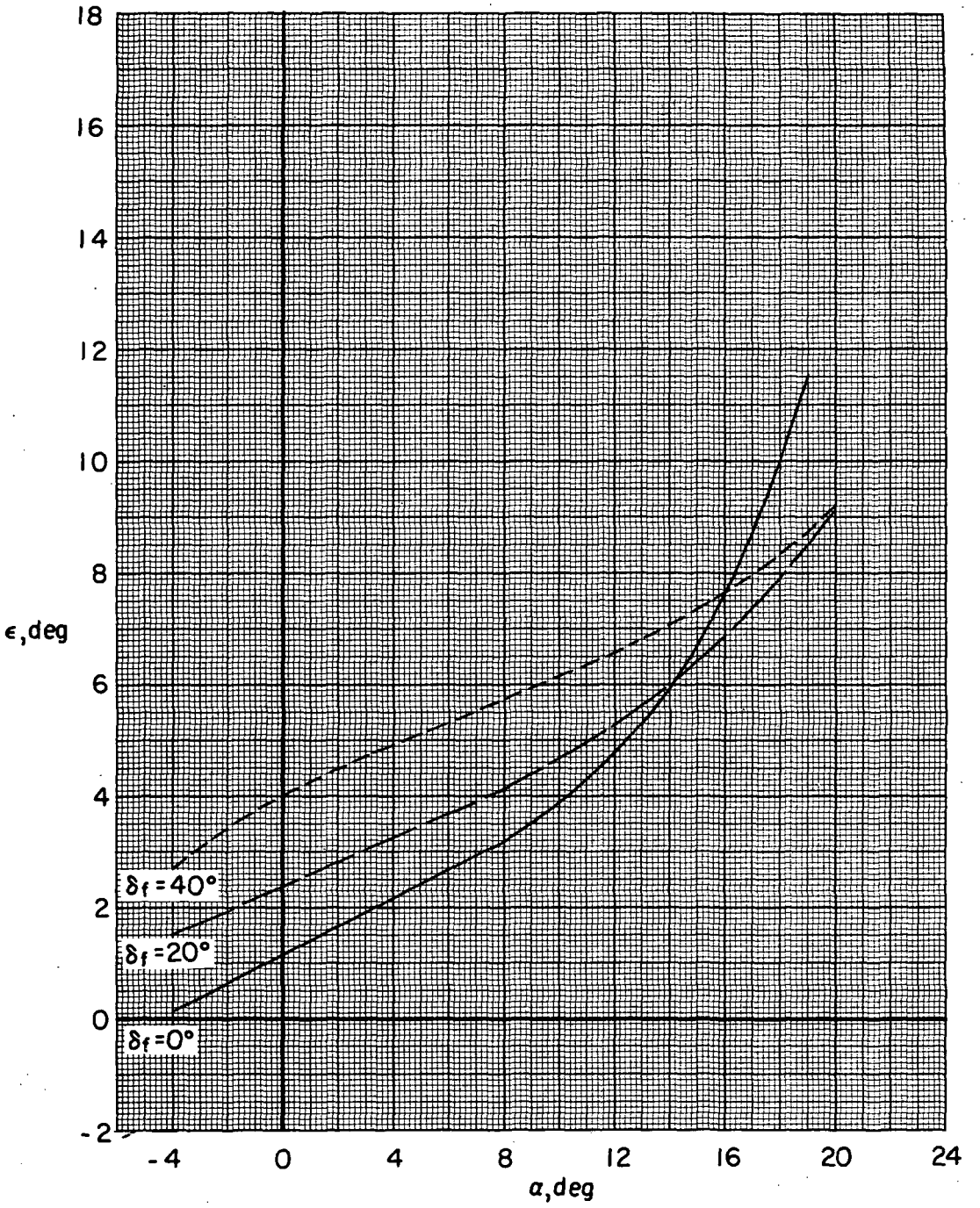

(a) Downwash angle.

Figure 19.- Effect of deflection of high-lift system on variation of effective downwash characteristics with angle of attack for model with nacelles off.

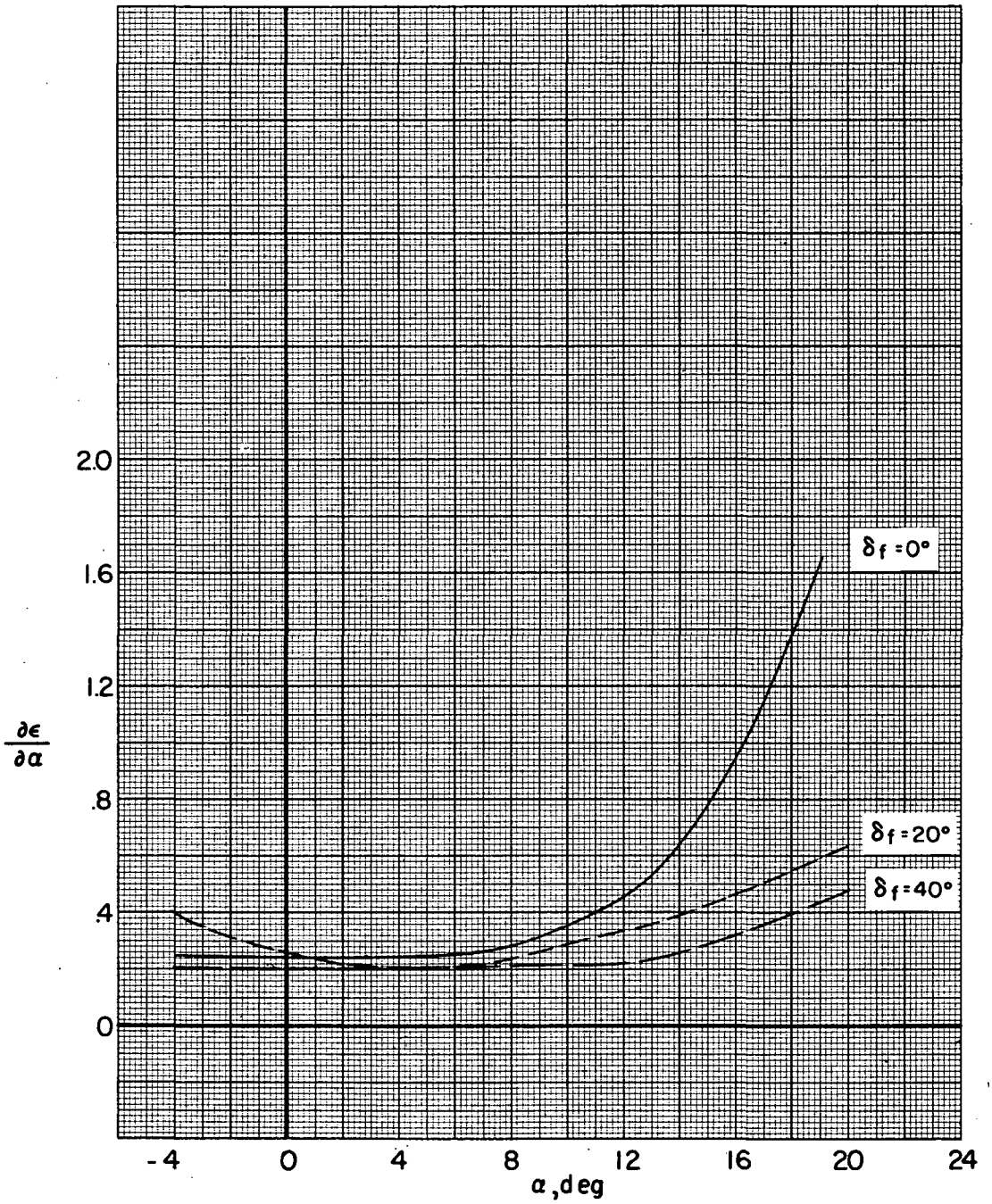

(b) Downwash slope, $\partial\epsilon/\partial\alpha$.

Figure 19.- Concluded.

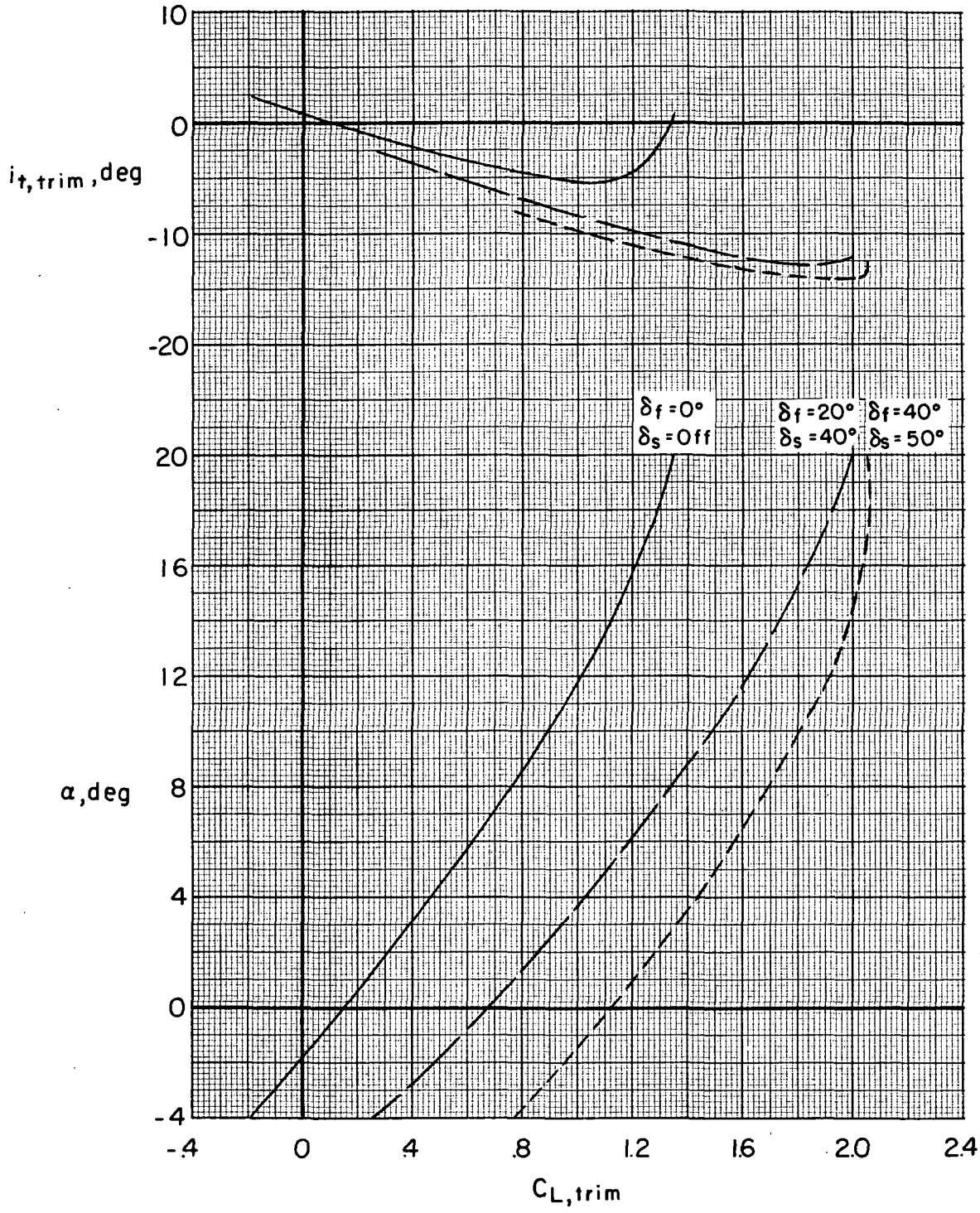

Figure 20.- Effect of deflection of high-lift system on variation of angle of attack and horizontal-tail setting for trim with trim lift coefficient for model with nacelles off.

NASA-Langley, 1972 — 1 L-8358

[redacted]

"The aeronautical and space activities of the United States shall be conducted so as to contribute . . . to the expansion of human knowledge of phenomena in the atmosphere and space. The Administration shall provide for the widest practicable and appropriate dissemination of information concerning its activities and the results thereof."

— NATIONAL AERONAUTICS AND SPACE ACT OF 1958

NASA SCIENTIFIC AND TECHNICAL PUBLICATIONS

TECHNICAL REPORTS: Scientific and technical information considered important, complete, and a lasting contribution to existing knowledge.

TECHNICAL NOTES: Information less broad in scope but nevertheless of importance as a contribution to existing knowledge.

TECHNICAL MEMORANDUMS: Information receiving limited distribution because of preliminary data, security classification, or other reasons.

CONTRACTOR REPORTS: Scientific and technical information generated under a NASA contract or grant and considered an important contribution to existing knowledge.

TECHNICAL TRANSLATIONS: Information published in a foreign language considered to merit NASA distribution in English.

SPECIAL PUBLICATIONS: Information derived from or of value to NASA activities. Publications include conference proceedings, monographs, data compilations, handbooks, sourcebooks, and special bibliographies.

TECHNOLOGY UTILIZATION PUBLICATIONS: Information on technology used by NASA that may be of particular interest in commercial and other non-aerospace applications. Publications include Tech Briefs, Technology Utilization Reports and Notes, and Technology Surveys.

Details on the availability of these publications may be obtained from:

SCIENTIFIC AND TECHNICAL INFORMATION OFFICE

NATIONAL AERONAUTICS AND SPACE ADMINISTRATION

Washington, D.C. 20546

[redacted]